

GEOLOGIC MAP OF THE COLOCKUM PASS SW AND SOUTHERN HALF OF THE NANEUM CANYON 7.5-MINUTE QUADRANGLES, KITTITAS COUNTY, WASHINGTON

by Andrew J. Sadowski, Amy L. Gilliland, and Megan L. Anderson

WASHINGTON
GEOLOGICAL SURVEY
Map Series 2021-03
December 2021

INTERNALLY REVIEWED



WASHINGTON STATE DEPARTMENT OF
NATURAL RESOURCES
WASHINGTON GEOLOGICAL SURVEY

GEOLOGIC MAP OF THE COLOCKUM PASS SW AND SOUTHERN HALF OF THE NANEUM CANYON 7.5-MINUTE QUADRANGLES, KITTITAS COUNTY, WASHINGTON

by Andrew J. Sadowski, Amy L. Gilliland, and Megan L. Anderson

WASHINGTON
GEOLOGICAL SURVEY
Map Series 2021-03
December 2021

*This geologic map was funded in part by
the USGS National Cooperative Geologic
Mapping Program, award no. G20AC00247*

*This publication has been subject to an iterative technical review
process by at least one Survey geologist who is not an author.
This publication has also been subject to an iterative
review process with Survey editors and cartographers.*



WASHINGTON STATE DEPARTMENT OF
NATURAL RESOURCES
WASHINGTON GEOLOGICAL SURVEY

DISCLAIMER

Neither the State of Washington, nor any agency thereof, nor any of their employees, makes any warranty, express or implied, or assumes any legal liability or responsibility for the accuracy, completeness, or usefulness of any information, apparatus, product, or process disclosed, or represents that its use would not infringe privately owned rights. Reference herein to any specific commercial product, process, or service by trade name, trademark, manufacturer, or otherwise, does not necessarily constitute or imply its endorsement, recommendation, or favoring by the State of Washington or any agency thereof. The views and opinions of authors expressed herein do not necessarily state or reflect those of the State of Washington or any agency thereof.

INDEMNIFICATION

Research supported by the U.S. Geological Survey, National Cooperative Geologic Mapping Program, under USGS award number G20AC00247. The views and conclusions contained in this document are those of the authors and should not be interpreted as necessarily representing the official policies, either expressed or implied, of the U.S. Government.

WASHINGTON STATE DEPARTMENT OF NATURAL RESOURCES

Hilary S. Franz—*Commissioner of Public Lands*

WASHINGTON GEOLOGICAL SURVEY

Casey R. Hanell—*State Geologist*

Jessica C. Czajkowski—*Assistant State Geologist*

Ana Shafer—*Assistant State Geologist*

Washington State Department of Natural Resources Washington Geological Survey

Mailing Address:

1111 Washington St SE

MS 47007

Olympia, WA 98504-7007

Street Address:

Natural Resources Bldg, Rm 148

1111 Washington St SE

Olympia, WA 98501

Phone: 360-902-1450

Fax: 360-902-1785

Email: geology@dnr.wa.gov

Website: <http://www.dnr.wa.gov/geology>

Publications and Maps:

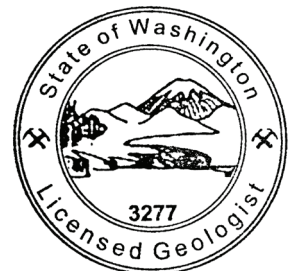
[www.dnr.wa.gov/programs-and-services/geology/
publications-and-data/publications-and-maps](http://www.dnr.wa.gov/programs-and-services/geology/publications-and-data/publications-and-maps)

Washington Geology Library Searchable Catalog:

[www.dnr.wa.gov/programs-and-services/geology/
washington-geology-library](http://www.dnr.wa.gov/programs-and-services/geology/washington-geology-library)



Suggested Citation: Sadowski, A. J.; Gilliland, A. L.; Anderson, M. L., 2021, Geologic map of the Colockum Pass SW and southern half of the Naneum Canyon 7.5-minute quadrangles, Kittitas County, Washington: Washington Geological Survey Map Series 2021-03, 1 sheet, scale 1:24,000, 23 p. text. [https://www.dnr.wa.gov/publications/ger_ms2021-03_geol_map_colockum_pass_sw_southern_naneum_canyon_24k.zip]



ANDREW JOHN SADOWSKI

Andrew Sadowski
Dec 2021

Contents

Introduction	1
Geologic Overview	2
Bedrock	2
Surficial Deposits	2
Tectonic Framework	2
Methods	2
Geologic Mapping	2
Data Collection and Analysis	3
Geochronology	3
Description of Map Units	3
Holocene to Pliocene Deposits	3
Holocene to Pliocene Alluvial Deposits	4
Tertiary Sedimentary and Volcanic Bedrock	5
Pre-Miocene Bedrock	12
Lithologies Depicted As Overlays	13
Mass Wasting (overlay mw)	13
Quaternary Loess (overlay Ql)	13
Miocene Hyaloclastite (overlay hy)	13
Discussion of Geologic Structures	13
West-Striking Faults	13
Northwest-Striking Faults	15
Northerly Striking Faults	15
Bend in Range Front	17
Blind Transtensional Faults	17
Folds	18
Water Resources in the Coleman member	19
Recommendations for Future Research	19
Acknowledgments	19
References	19
Appendix A. Detrital Zircon Separation and Analytical Methods	23

FIGURES

Figure 1. Reference map of geologic structures in northern Kittitas Valley	14
Figure 2. Geophysical interpretation for the map area showing filtered data	16

TABLES

Table 1. U-Pb geochronology of detrital zircons from the Ellensburg Formation	6
Table 2. Main characteristics of the units of the Columbia River Basalt Group	8

MAP SHEET

Geologic Map of the Colockum Pass SW and Southern Half of the Naneum
Canyon 7.5-minute Quadrangles, Kittitas County, Washington

Figure M1. Geophysical interpretation for the map area

Geologic Map of the Colockum Pass SW and Southern Half of the Naneum Canyon 7.5-minute Quadrangles, Kittitas County, Washington

by Andrew J. Sadowski¹, Amy L. Gilliland¹, Megan L. Anderson¹

¹ Washington Geological Survey
1111 Washington St SE
MS 47007
Olympia, WA 98504-7007

ABSTRACT

New geological and geophysical investigations of the Colockum Pass SW and Naneum Canyon quadrangles characterize geologic structures and the basin architecture of northeastern Kittitas Valley. New 1:24,000-scale mapping identifies oblique-slip and reverse faults, fault-related anticlines, and long monoclines. Strain transfer between west-striking and northwest-striking faults occurred—or is occurring—near a bend in the range front. Forward modeling of gravity and aeromagnetic data constrains our interpretations of fault and fold geometries, identifies a blind, pipe-like mafic intrusion, and suggests relict, blind, transtensional sub-basins containing—and concealed by—Miocene bedrock.

Our mapping refines bedrock and surficial stratigraphy near the northern extent of the Miocene Columbia River Basalt Group (CRBG). Whole rock geochemistry identifies the Mount Horrible, Wapshilla Ridge, Grouse Creek, Ortley, and Sentinel Bluffs members of the Grande Ronde Basalt (GRB of CRBG) and the overlying Frenchman Springs and Priest Rapids members of the Wanapum Basalt. The Ortley member is a locally invasive flow containing peperitic hyaloclastite. The Coleman and Vantage members of the sedimentary Ellensburg Formation are interbedded in the CRBG, where unconformities exist between the Vantage member, the Wanapum Basalt, and the upper Ellensburg Formation. Three new detrital zircon U-Pb analyses identify the maximum depositional ages (MDA) of these sedimentary members. With these MDAs, we calculate a minimum tilting rate in the southern map area of approximately 1 degree per million years recorded in Miocene bedrock.

Lidar elucidates alluvial fans, landslides, and fault escarpments. The Coleman member and other interbeds exhibit areas prone to landslides at the surface and suggest zones of potential aquifers at depth.

INTRODUCTION

The Colockum Pass SW and southern half of the Naneum Canyon 7.5-minute quadrangles (herein also referred to as “the map area”) are located in east-central Kittitas County, Washington. The map area covers the northern portion of Kittitas Valley, located east of the Cascade Range, on the western edge of the Columbia Basin. Most of the low-lying lands in the map area are used for agriculture; higher elevations are a mix of private residential land and the Okanogan–Wenatchee National Forest. The lowlands slope very gently to the south, with low hills (less than ~150 ft tall) at several locations. These low hills are aligned in rows in many places and are composed of bedrock or older alluvium. Numerous long, linear south-flowing creeks drain deep canyons in the northern map area, including (from west to east): Wilson, Naneum, Coleman, and Cooke creeks. The deep, narrow canyons bear the same names as the creeks that drain them. Other deep, narrow canyons include: Cave, Schnebly, and Dawson canyons. The northern range front of Kittitas Valley

bends southward in the eastern map area. Numerous active and inactive rock quarries that mine basalt or gravel are scattered throughout the map area.

To better understand geologic hazards (earthquakes, landslides, debris flows) and natural resources (water, aggregate), our 1:24,000-scale geologic map builds upon prior geologic mapping at 1:100,000 scale (Waitt, 1979; Tabor and others, 1982) and adjacent 1:24,000-scale mapping (Sadowski and others, 2020). Our mapping also identifies stratigraphy similar to detailed geologic mapping by Hammond (2013) that is southwest of the map area near the Naches River. Our work is part of a multi-year geologic mapping project to characterize active faults in the region and better understand how the Yakima fold and thrust belt (YFTB) may transfer strain across the Cascade Range. In this map area we continued mapping structures that project eastward from the adjacent map area of Sadowski and others (2020) (Ellensburg North and Reecer Canyon quadrangles). The mapping will

assist in geologic hazard assessment, geotechnical engineering, groundwater hydrology, earth resource management, academic research, and investigations for growth management planning.

GEOLOGIC OVERVIEW

Bedrock

The oldest rocks exposed in the map area are basaltic andesite of the Miocene Grande Ronde Basalt (GRB) of the Columbia River Basalt Group (CRBG), a continental flood basalt province (Reidel and Tolan, 2013). Roughly 95 percent of the CRBG erupted rapidly between 16.7 and 15.9 Ma (Kasbohm and Schoene, 2018). The GRB constitutes about 72 percent of the CRBG formations by volume (Reidel and others, 2013a). The oldest exposed CRBG member in the map area is the Mount Horrible member, located in the northwest portion of the map. The youngest exposed CRBG member in the map area is the Priest Rapids Member of the Wanapum Basalt, which is located in the southeastern corner of the map.

Volcaniclastic and feldspathic sedimentary rocks of the Ellensburg Formation overlie, interfinger, and underlie the GRB (Schmincke, 1964, 1967; Smith, 1988a,b). The two general sources for these sedimentary rock types are recognized as (1) the ancestral Cascade Range that provided volcaniclastic detritus to the ancestral Columbia Basin, and (2) ancient rivers of the inland Pacific Northwest (such as the ancestral Columbia River) that provided the feldspathic material to the ancestral basin from distal sources (Schmincke, 1964, 1967; Smith 1988a,b). The Coleman member—informally named by Bentley (1977)—is a mappable interval within the Ellensburg Formation and is identified in Coleman Canyon. The Coleman member of the Ellensburg Formation is an extensive, micaceous interbed that overlies the Grouse Creek and Ortley members and underlies the Sentinel Bluffs Member of the GRB.

Surficial Deposits

Miocene bedrock is unconformably capped with Pliocene through Holocene nonglacial deposits. Porter (1976) and Waitt (1979) mapped glacial, glaciofluvial, and nonglacial deposits in detail to the west of and within the map area, respectively. We mapped alluvium and alluvial fan deposits of various ages and considered whether they could be distal alpine glaciofluvial outwash from the northern uplands that include the Wenatchee Mountains, though we didn't see clear evidence for Quaternary alpine ice in the map area. This is especially the case for the Pliocene Thorp Gravels and other Plio-Pleistocene gravels. For these accumulations, we follow the depositional environment interpretations of Waitt (1979) and Sadowski and others (2020), respectively. We divide the alluvial terraces based on relative ages inferred from differences in elevation and surface morphologies using lidar data, and not based solely on provenance (for example, polymict clasts that are sourced from the Cascade Range via mainstream outwash channels or monomict clasts that are locally sourced from sidestream outwash pathways).

While Pleistocene eolian loess of the Palouse Formation is prevalent in eastern Washington, the loess is irregularly distributed in the Kittitas Valley. The sediment source for loess

was the wind-blown redistribution of fine-grained sand and silt of slackwater deposits from cataclysmic floods related to continental glaciations (McDonald and Busacca, 1992). Landslide deposits and mass-wasting landforms drape older units and are identified using field- and lidar-informed observations. The youngest surficial units in the valley—and, where applicable, their channel networks—are extensively modified by agriculture, irrigation, and aggregate mining.

Tectonic Framework

The map area lies within the modern backarc of the Cascadia subduction zone. During the Paleogene, extensional and transtensional structural basins filled with non-marine Eocene sediments and volcanic rocks (Tabor and others, 1982; Johnson, 1985; Eddy and others, 2016, 2017). These continental basins were later filled and capped by voluminous Neogene lavas during the onset of Miocene compression and transpression. This stress regime resulted from oblique subduction with steady, regional, clockwise rotation of the crust (Reidel and others, 1984; Wells and McCaffrey, 2013; Brocher and others, 2017). Global Positioning System (GPS) velocities show ongoing north–northeast-directed shortening (McCaffrey and others, 2013; Wells and others, 1998). Extensive, kilometer-scale, west- and northwest-striking, reverse-to-thrust faults and associated folds of the YFTB accommodated deformation (Reidel and others, 2013b; Kelsey and others, 2017; Staisch and others, 2018a,b). The map area encompasses the northern extent of the YFTB from Kittitas Valley to the Wenatchee Mountains (Rosenmeier, 1968; Tabor and others, 1982). Miocene units are subhorizontal and flat-lying in the Wenatchee Mountains to the north, and are tilted progressively steeper southward toward Kittitas Valley.

METHODS

Geologic Mapping

We identified lithologic units from field observations in the summer and fall of 2020. Field data were collected using traditional geological field methods and digitally recorded in the field with Esri's ArcGIS Field Maps application. We reviewed prior geologic mapping at 1:100,000 scale (Waitt, 1979; Tabor and others, 1982), recent aerial orthophotos, and elevation data from lidar (FEMA, 2011; PSLC, 2011; Eylon International 2014a,b; UNAVCO, 2014; WA DNR, 2018a,b). Lidar data were used to derive hillshade images, contours, red relief image maps (Chiba and others, 2008), and other terrain products. We mapped flood basalt volcanic texture, generally found in the following order (from bottom to top)—hyaloclastites of pillow-palagonite breccias, basal colonnades, entablatures, internal vesicular zones, vesicular tops, and autobreccias (Reidel, 2015). The physical volcanology of the flows helped us assess the flow-by-flow stratigraphy and choose samples to analyze for whole rock geochemistry that would elucidate the chemostratigraphy of the flows (Reidel, 2005; Reidel and Tolan, 2013; Sadowski and others, 2020). Bedding attitudes, sedimentary structures, igneous foliations, joints, and shears in bedrock were measured and recorded where we were confident that these features were in place. In CRBG rocks, planar orientations of flow foliation surfaces were measured on

vesicular and colonnade tops. Similarly, the orientations of column sides in colonnade sections were also measured and analyzed stereographically using Stereonet 10.1.0 software (Allmendinger and others, 2012; Cardozo and Allmendinger, 2013) to determine cooling surfaces inferred to represent paleo-horizontal.

In general, we symbolize confidently identified and accurately located fault scarps with solid lines and their respective fault symbols on the geologic map (Map Sheet), whereas we map and symbolize escarpments of unknown origin with hachured lines where we are less confident of a purely tectonic origin. These escarpments of unknown origin may be breaks in slope of surficial units (Quaternary or older). We could neither confirm nor refute that these escarpments are tectonic in origin despite many being subparallel to existing faults.

Data Collection and Analysis

We reviewed multiple datasets in support of our mapping: well logs, boring records, geotechnical reports, geophysical data (gravity and aeromagnetism), geochemical analyses (major element and trace element), petrographic analysis of thin sections, and identification of geomorphic features using lidar. More than 70 water wells, geotechnical borings, and oil and gas wells were reviewed to inform subsurface understanding.

POTENTIAL-FIELDS GEOPHYSICAL METHODS

We collected new gravity data using a Scintrex model CG-6 gravimeter. Grid spacing is 1–2 km (3,281–6,562 ft) with profile lines at 250-m (820 ft) spacing. Gravity data are referenced to the International Gravity Standardization Net of 1971 (Morelli and others, 1974). Isostatic anomalies result from applying Bouguer, Earth curvature, and terrain corrections to 166.7 km using the standard reduction density of 2,670 kg/m³, a 25-km-thick crust at sea level, and a crust-mantle density contrast of 400 kg/m³ (Heiskanen and Vening-Meinesz, 1958; Jachens and Roberts, 1981; Telford and others, 1990; Swick, 1942). A horizontal gradient filter applied to the isostatic gravity grid helped identify linear gravitational gradients, commonly associated with steeply dipping contacts or with faults, where stronger gradients usually imply more extreme deformation. Aeromagnetic data from two surveys (Blakely and others, 2020a,b) reveal magnetic anomalies related to volcanic bedrock and highlight lineaments possibly related to faults or folds.

Forward modeling of the potential-field anomalies along Cross Section A–A' using GM-SYS (Geosoft, Inc.) helped constrain possible bedrock geometries in the subsurface. In addition to published rock properties (Staisch and others, 2018a,b), more than 60 density and magnetic susceptibility measurements from samples collected within and beyond the map area provide guidance for our modeling parameters for local geologic units. General CRBG thicknesses and the top of the CRBG within Kittitas Valley at the southern end of our model agree with models by Staisch and others (2018a) and Kelsey and others (2017) in nearby areas.

GEOCHEMISTRY

A total of 166 samples constrain whole rock major and trace element composition and were analyzed at the Peter Hooper GeoAnalytical Laboratory at Washington State University (WSU) in Pullman. X-ray fluorescence (XRF) via inductively coupled plasma atomic emission spectroscopy (ICP-AES) provide major element compositions and inductively coupled plasma mass spectroscopy (ICP-MS) provide trace element compositions (*Data Supplement Table DS01*). Geochemical analyses of samples from the crystalline cores of lavas (colonnades and entablatures) give the most representative compositional results. If neither were available, then samples from vesicular tops sufficed, with a caveat being that geochemistry from the oxidizing, cooling surface of a lava flow may be geochemically less representative than the core of the flow. Geochemical results were assessed using compositional variation diagrams—primarily TiO₂–MgO and TiO₂–P₂O₅—and classified accordingly into CRBG sub-members using a machine learning (ML) model developed by Ashley Steiner at WSU. Note that geochemistry sites G01–06 reside outside of the map area and these are numbered clockwise from north through east.

Geochronology

U–Pb analysis of detrital zircon grains extracted from three samples in the map area provide new information about sediment provenance and depositional age for units within the Ellensburg Formation and sediments of Pliocene–Pleistocene gravels. Approximately 7 kg of sample were collected and sent to ZirChron LLC for separation. Zircon separates were analyzed by Vic Valencia and Jeff Vervoort at the Radiogenic Isotope and Geochronology Lab (RIGL) at WSU. We targeted ~100 grains per sample. Detailed method descriptions are in *Appendix A* and analytical results in the *Data Supplement (Tables DS02A through DS02C)*. From these data, we interpret a maximum depositional age (MDA), where the age of the deposit must be younger than or equal to the MDA. Depending on the geologic context of the sample and the source area, we interpret the MDA as an average of the youngest population of grains where geologic context suggests that it represents a single igneous event; otherwise, we use the youngest single age. Where deposition is more continuous than a single event, such as fluvial deposition of detrital zircons, the youngest single grain is used in our study.

DESCRIPTION OF MAP UNITS

Holocene to Pliocene Nonglacial Deposits

- | | |
|----|--|
| af | Artificial fill (Holocene) —Rubble of introduced material; cobbles, pebbles, sand, and boulders; poorly sorted and unconsolidated; used for home sites or infrastructure. |
| ml | Modified land (Holocene) —Rubble of local material; sand- through boulder-sized material is redistributed to modify topography and form graded landscapes for industrial, agricultural, and residential zones, including but not limited to gravel pits, rock quarries, and home sites. |

Qp Peat (Holocene to Pliocene)—Peat deposits and ephemeral waterbodies; organic and organic-rich sediment; unit includes peat, gyttja, muck, silt, and clay; typically in closed depressions; mapped in wetland and bog areas and distinctly flat-bottomed depressions; also mapped from evaluation of aerial photos where black to dark gray ephemeral ponds and water bodies were not mapped in the published base map. The thickness of most peat deposits is largely unassessed but presumed to be less than 30 ft. Small peat deposits are scattered throughout the map area, typically within alluvium and related to ponding of stagnant water.

Qls Landslide deposits (Holocene to Pliocene)—Clastic aggregate; medium brown, weathering is typically mild; generally loose, jumbled, and poorly consolidated; clay- to boulder-sized clasts; angular to subrounded; unsorted, matrix-supported; unstratified and structureless; unit contains rubble of sand, silt, clay, cobbles, pebbles, boulders, and diamicton of basalt and sandstone of varied amounts; deposit thicknesses are less than 100 ft and typically less than 50 ft; unit is generally restricted to the uplands along steep canyon walls, the flanks of topographic saddles north of the range front, and near and downslope from the Ellensburg Formation (unit **Mce**) and its Coleman member (unit **Mcec**). Notably, the large landslide complex between Schnebly and Charlton canyons likely has a slide plane associated with the Coleman member. Here, slopes of exposed basalt of McCoy Canyon (unit **Mvgsmc**) slid upon the concealed Coleman member underlying the basalt. Likewise, the west side of Coleman Canyon in the northern map area likely contains many landslides related to the concealed Coleman member. Farther up Naneum Canyon, there are more landslide deposits likely resulting from a bedrock transition from competent Miocene basaltic andesite to less competent Eocene sandstone (Swauk Formation?). Deposits are identified as having “crisp” landform morphologies that exhibit sharply defined lineaments on lidar, representing scarps, blocks, and cracks of landslides and landslide complexes. A mass-wasting overlay (**mw**) is also used to delineate landforms with landslide-like characteristics (such as hummocky topography) that are difficult to characterize as landslide deposits. These suggest mass movement where evidence for landslide deposits is inconclusive. Precise ages and recurrences of deposits are unknown.

Qlso Old landslide deposits (Pleistocene to Pliocene)—Clastic aggregate; medium brown to light yellowish brown; poorly consolidated; clay- to boulder-sized clasts; angular to subrounded; unsorted, matrix-supported; unstratified and structureless rubble; older landslide deposits are identified as having smoother, muted landform morphologies on lidar compared to “crisper” landform morphologies (see unit **Qls**) that

are interpreted to be relatively younger. Deposits of unit **Qlso** are generally geographically larger than unit **Qls**. Unit **Qlso** is only exposed in the northern reaches of Naneum Canyon. Precise ages and recurrences of these deposits are unknown.

Holocene to Pliocene Alluvial Deposits

Stream channel and stream flood (overbank) deposits and terraces. Deposits include pebbles, cobbles, sand, silt, clay, peat, and boulders, all in varying amounts and thicknesses. Colors range from light tannish gray to medium brown. The deposits are fresh to mildly weathered, not compacted or cemented, and include mostly sand and gravel. The grains are typically well rounded, moderately to well sorted, and basaltic (monomict). Deposits are as follows:

Qa Alluvium (Holocene)—Stream channel deposits on active flood plain; unit is narrowly distributed throughout the lowest elevations of the map area and common in the channels of Wilson, Naneum, Coleman, and Cooke creeks; depositional environment is an active flood plain; areas of this unit have been heavily modified by agricultural cultivation and have map patterns that reflect such modification, such as sharp angles. Precise ages of unit **Qa** are unknown.

Qia Intermediate-aged alluvium (Holocene to Pleistocene)—Stream flood (overbank) and old channel deposits near active flood plain; unit is the most widespread deposit by area and is widely distributed in the lower portions of the south-central map area; surfaces of unit **Qia** are slightly elevated relative to surfaces of unit **Qa**. Unit **Qia** is sometimes indistinguishable from alluvial fan unit **Qaf1** based on lithology, but tends to be found in closer proximity to unit **Qa** and at lower elevations than unit **Qaf1**. Precise ages of unit **Qia** are unknown.

Qaf Alluvial fan deposits (Holocene to Pleistocene)—Alluvial fan and debris flow deposits composed of unconsolidated to poorly consolidated sand and gravel; colors range from various shades of brown to brownish medium gray; weathering rinds vary from less than 1 mm up to 1 cm; not compacted; silt- to boulder-sized clasts; angular to subrounded; unsorted; clast composition depends on the composition of bedrock from which the unit is derived but is generally basalt; unit thickness varies with age, where older units tend to be thicker but are generally less than 50 ft; Quaternary fan surfaces are generally locally derived from the CRBG. These fan-like deposits are likely alluvial in origin because evidence of glacial ice is ambiguous in the northern portions of the map area east of Wilson Creek and in Naneum Basin.

Unit is subdivided and numbered from 1 (lowest and youngest) to 4 (highest and oldest) based on relative elevation above the modern stream level and differences in surface morphologies. Precise ages for the units

are unknown. Older surfaces are smoother and more deeply incised compared to rougher, younger surfaces with lesser degrees of fluvial incision. Weathering rinds are <1 mm on unit Qaf₁, about 1 mm on units Qaf₂ and Qaf₃, and >1 mm on unit Qaf₄. Loess is generally absent on younger surfaces and common on older surfaces. Notably, escarpments related to the Dead Coyote fault are common and sharp within units Qaf₃ and QRcg. Large fan surfaces may be attributed to either alluvial processes or glaciofluvial outwash processes, but because there are no clear indications of glacial deposits associated with these fans, we interpret them to be alluvial in origin. Silicic caliche (hardpan) is more common on older units Qaf₃ and Qaf₄. Good examples of numerous generations of alluvial fans are on and northeast of a series of northwest-trending low hills between Naneum and Fairview Roads and north of Brick Mill Road.

QRcg

Oldest alluvium (Pleistocene to Pliocene)—Basaltic gravel and sand; yellowish light brown to dark brown, moderately to strongly weathered with weathering rinds greater than 1 mm and up to a few centimeters thick; moderately compacted; cobbles and pebbles; well rounded to rounded; moderately to well sorted, clast supported; imbrications of clasts suggest southward (SSE–SSW) paleocurrent directions away from Naneum and Cooke canyons; basalt dominant, composed of GRB; unit thickness is variable; south of the southern splay of the Dead Coyote fault, unit is on the order of hundreds of feet thick in the basin. Unit is common in the eastern, central, and southern zones of the map area in Kittitas Valley. Large portions of these deposits may have originated as debris flows (from breached landslide-dammed lakes?) tentatively sourced from the north from either (a) Naneum basin via Naneum Canyon, which would suggest right-lateral translation of the deposit because the unit is west of this canyon, and there are oblique-slip faults nearby, and (or) possibly (b) from the smaller Wilson Creek canyon. Unit is highly elevated above other alluvial fan deposits, and thinly drapes over bedrock near the range front. The large surface near Naneum Canyon has steep western slopes in the adjacent map area (Sadowski and others, 2020) and gentle eastern slopes in the map area. Loess is extremely pervasive on these surfaces and thin (<1 ft), discontinuous siliceous caliche layers are common in the near surface. Shallow, poorly confined to unconfined groundwater flows above, between, and below these caliche layers (Owens, 1995). Escarpments of the Dead Coyote fault are common and subtly visible within this unit. Unit was previously mapped as the side stream facies of Thorp Gravel by Waitt (1979), and previously referred to as “Naneum Gravel” in field trip guides for the Kittitas Valley by Bentley (1977). Unit is contemporaneous with or younger than Thorp Gravel and it is unclear if these two units have similar origins. Unit QRcg is very similar looking to units Qaf₄ and Mc_e and could be mistaken for these. Where

age control is available, U-Pb age spectra from detrital zircons distinguish unit QRcg from the older unit Mc_e. Unit QRcg is distinguished from unit Qaf₄ by location, where unit Qaf₄ is generally restricted to areas near the range front and unit QRcg is more distal from the range front with possible lateral continuity. We speculate that units QRcg and Qaf₄ may overlap in age, but we have no age control on unit Qaf₄ to support this notion.

Tertiary Sedimentary and Volcanic Bedrock

SEDIMENTARY ROCKS OF THE ELLENSBURG FORMATION

Mc_e Ellensburg Formation, undivided (Miocene)—Volcaniclastic to lacustrine or fluvial sedimentary bedrock underlying, intercalated with, and overlying rocks of the CRBG; light to medium brown to light to medium gray; mildly to strongly weathered; moderately to well-indurated; medium-grained; subangular to subrounded; well to moderately sorted; grain supported; sand composition of feldspar, quartz, and lithic fragments ($F \geq Q > L$) includes potassium feldspar (25%, orthoclase + microcline), plagioclase (5–15%), quartz (25–30%), basalt lithic fragments (3–10%), and mica (<4%, <0.75 mm, white, clear, muscovite); thickness is generally less than 300 ft; exposures can vary from thin, discontinuous, poorly exposed interbeds in the GRB or above the CRBG with lighter color tones on aerial imagery to well-exposed contiguous outcrops along cliffs, topographic saddles and benches, and ditches; as intercalated interbeds in GRB, unit can be commonly identified where vegetation preferentially grows from sedimentary soils with higher permeability rather than basalt; unit commonly crops out near and above landslides. We ascribe a genetic relationship between landslides and incompetent sedimentary layers of the Ellensburg Formation, where these layers act as slide planes for more competent basaltic bedrock to fail and produce mass-wasting landforms and landslide deposits. Thin (<1 ft) siliceous caliche layers are common and discontinuous in the near surface. Unit locally and unconformably overlies the Priest Rapids member of the Wanapum basalt. New U-Pb analysis of detrital zircons for post-Wanapum deposits of the Ellensburg Formation yields an MDA $\leq 5.76 \pm 0.36$ Ma (age site GD03, Table 1, *Data Supplement Table DS02c*). Unit Mc_e is generally mapped where we lack outcrop exposures and infer interbeds according to colluvial float or landform morphology such as topographic benches. Where outcrops are available, unit is divided based on grain size or based on stratigraphic relationship to known members of the CRBG (such as Vantage or Coleman sedimentary units):

MCev Vantage member of the Ellensburg Formation (Miocene)—Pumiceous sandstone; light brownish gray, moderately to strongly weathered; mildly to moderately indurated, mildly cemented; relative proportions of subangular grains are greater than angular grains; fine- to medium-grained; poorly sorted, matrix-supported; sand composition is variable ($F \gg Q \gg L$ to $L > F > Q$) and includes plagioclase (10–15%), potassium feldspar (0–3%), quartz (5–20%), and lithic fragments (<20%); lithic fragments are generally volcanic and pyroclastic (pumice, 0.5 mm–2.0 cm, white), porphyritic, and may be basaltic(?); sand composition generally lacks mica. The pumice fragments are very common, easily visible, and distinctive for this unit. Unit thickness is greater than 100 ft. The unit is located in the southeastern corner of the map area and east of Caribou Road. Depositional environment is presumed to be terrestrial paleotopographic lows such as a lake. The unit unconformably overlies the GRB in and around Kittitas Valley and we infer it doing so in the southeast corner of the map area as well. New U-Pb analysis of detrital zircons yields an MDA of $\leq 14.77 \pm 0.38$ Ma (age site GD02, Table 1, *Data Supplement Table DS02b*). Reference localities include age site GD02 and northeast of water well W22, both of which are in the southeast corner of the map area.

MCec Coleman member of the Ellensburg Formation, undivided (Miocene)—Sandstone and siltstone underlying the Sentinel Bluffs Member and overlying the Ortley member of the CRBG. Informally named by Bentley (1977) near Coleman Canyon of northern Kittitas Valley and mapped by Hammond (2013) as far south as the Naches River area. It is equivalent to the eponymous Rock Island member of Hoyt (1961) farther north, the Douglas Creek member of Ebinghaus and others (2015), and the Rock Island arkosic sands of

Schmincke (1967). Unit is generally a micaceous, medium-grained sandstone with poorly to moderately cemented grains. Less than 200 ft thick of well-exposed sedimentary outcrop is observed. Unit is commonly exposed in Coleman Canyon between Schnebly and Cooke Canyons at its eastern extent, in Reecer Canyon at its western extent, and in topographic saddles between those, particularly north of the range front on either side of Naneum Canyon. These exposures are commonly in the mid-to-low elevations of the map area. Depositional environment is assumed to be a Miocene fluvial and (or) lacustrine setting in Miocene paleotopographic lows. Unit is consistently mapped between the GRB Ortley member (unit **Mvgo**) and the basalt of McCoy Canyon (unit **Mvgsmc**) in the map area, whereas mapping in the westward adjacent map area (Sadowski and others, 2020) mapped the unit between the Grouse Creek (unit **Mvgg**) and the basalt of McCoy Canyon members (unit **Mvgsmc**). These contact relationships suggest that the Coleman member is not a discrete lithological horizon such as a bed but is an interval. Hyaloclastite—with or without siltstone—irregularly underlies the Coleman member and can indicate proximity to the Coleman member. Landslides are common downslope of Coleman member exposures, and we ascribe a genetic relationship between these sedimentary interbeds and landslide deposits. Although we did not map the Coleman member up Schnebly Canyon or in the northwestern map area, large landslide complexes spanning the Ortley member and the basalt of McCoy Canyon may be related to blind interbeds of the Coleman member. New U-Pb analysis of detrital zircons yields an MDA of $\leq 15.33 \pm 0.35$ Ma (age site GD01, Table 1, *Data Supplement Table DS02a*). Although the youngest single grain of this sample is 6.49 ± 0.41 Ma, this is geologically untenable because the sample is interbedded in the

Table 1. U-Pb geochronology of detrital zircons from the Ellensburg Formation (unit **MCe**). MDA stands for Maximum Depositional Age.

Site	Name	Lithology	Unit	MDA	Method
GD01	Coleman mbr	Siltstone	MCec	$\leq 15.33 \pm 0.35$ Ma	Youngest single grain*
GD02	Vantage mbr	Pumiceous sandstone	MCev	$\leq 14.77 \pm 0.38$ Ma	Youngest single grain
GD03	Upper Ellensburg Fm	Sandstone lense in cobble gravel	MCe	$\leq 5.76 \pm 0.36$ Ma	Youngest single grain

*A single ~6.5 Ma grain found in this sample is geologically impossible because the sample is situated between two Middle Miocene basalts (~15–16 Ma) and therefore does not represent the MDA. The next youngest grain is what is reported in the table.

GRB, which is older, and the young grain could be sample contamination. Therefore we report the next youngest single grain (15.33 ± 0.35 Ma). The Coleman member may form an aquifer at depth in the Kittitas Valley. Unit thickness is poorly constrained at depth, and geophysical modeling suggests greater thickness in Kittitas Valley compared to what we observe at the surface in the range front. The Coleman member is divided into subunits based on grain size:

MCsec Sandstone of the Coleman member (Miocene)—Micaceous feldspathic sandstone; medium brown, yellowish brown to light tan, moderately to strongly weathered; mildly to moderately indurated; poorly to moderately cemented, mildly to moderately indurated, well consolidated; generally medium-grained sand, but can range from fine- to coarse-grained sand; relative proportions of subrounded grains are greater than subangular grains; well-sorted, grain-supported; generally structureless with uncommon planar, parallel laminations; approximate mineral composition of the sand grains is $Q \geq F \gg L$; quartz (20–40%), potassium feldspar (10–20%), mica (1–12%, 0.5–1 mm, white-clear, muscovite); thickness is less than 250 ft, although geophysical modeling suggests a greater thickness at depth; depositional environment is inferred to be fluvial or lacustrine (Smith, 1988a,b); unit is located between the Ortley member (unit **Mvgo**) and the basalt of McCoy Canyon (unit **Mvgsmc**) of the Sentinel Bluffs Member; good exposures can be found in roadside exposures between Dawson Road and Coleman Creek Road in the northeastern map area, in topographic saddles behind faceted spurs of the range front east of Naneum Canyon, and at a reference locality at a road bend under a powerline corridor between geochemistry sites G095 and G068.

MCfec Siltstone of the Coleman member (Miocene)—Micaceous siltstone;

gray to brown, moderately to strongly weathered (weathered to clay where strongly weathered); lightweight, low density, poorly indurated to friable, mildly cemented; silt to fine-grained sand; relative proportions of subangular grains are greater than subrounded grains; well-sorted, matrix-supported; silt composition is difficult to assess but includes plagioclase feldspar and mica (<10%, <0.05 mm, clear to white, muscovite) and may include potassium feldspar; unit thickness is generally less than 200 ft; unit is located in the northeastern map area, interbedded between basalts of the Sentinel Bluffs member (in or above unit **Mvgssf**); a lacustrine or fluvial depositional environment is inferred (Smith, 1988a,b); contacts may pinch out over short distances.

VOLCANIC ROCKS OF THE COLUMBIA RIVER BASALT GROUP (CRBG)

Volcanic rocks of the CRBG are geochemically classified as basaltic andesite to basalt. In general, they are very dark gray to medium gray where fresh, and medium to dark brown where weathered. Weathering is moderate. These rocks are dense and hard. Their textures are aphyric, generally aphanitic, where crystals in the groundmass can vary from ~0.1 mm to a few millimeters, uncommonly microporphyritic, and rarely porphyritic. Flows commonly exhibit the following physical characteristics: basal, columnar-jointed colonnades, interior entablatures, and capping vesicular flow tops. Many volcanic units of the CRBG are comprised of multiple flows, and contacts between flows of the same unit are separated by solid or dashed form lines on the Map Sheet. Flows of the CRBG are locally divided into the following units, where flows are named following Reidel and Tolan (2013).

Where whole rock geochemistry was available (*Data Supplement Table DS01*), a machine learning (ML) model developed at Washington State University's (WSU) GeoAnalytical Laboratory quickly classified samples into established CRBG stratigraphy before using compositional variation diagrams. Table 2 summarizes the characteristics of the mapped CRBG units. This table includes the approximate unit thicknesses, textures, crystal sizes, the percentages, sizes, and relative abundances of mafic minerals, approximate ranges for elemental compositions (TiO_2 , MgO , P_2O_5 , Zr), and magnetic remanences. As such, the CRBG is geochemically divided in the map area into:

Mvwp Priest Rapids Member of Wanapum Basalt (Miocene)—Basalt; dark gray to grayish brown; well indurated; mostly microporphyritic with crystal sizes ranging from medium to coarse (0.3–1.1 mm), less

Table 2. Main characteristics* of the units of the Columbia River Basalt Group (CRBG) in Colockum Pass SW and southern half of Naneum Canyon 7.5-minute quadrangles, northern Kittitas Valley.

Unit label	M _{VWP}	M _{VWF}	M _{Vgsm}	M _{Vgssc}	M _{Vgssf}
Unit thickness (ft)	~ 300, top not exposed	< 200	> 100, top not exposed	< 250	> 250
Texture	microporphyritic (to aphyric)	microporphyritic (to aphyric)	aphyric, aphanitic	aphyric, aphanitic	aphyric, aphanitic
Crystal size (mm)	0.3–1.1	0.75–1.2	0.10–0.12, max 0.55 mm	0.1–0.5, max 1.75 mm	0.7–0.55
Mafic minerals (% , size, abundance)	15–20%, 0.1–0.5 mm, ol + cpx	20–30%, 0.3–0.5 mm, ol + cpx > opx	2–10%, ~0.05 mm, rarely as large as 0.3 mm, cpx > ol	10–30%, ~0.1–0.2 mm	< 20%
Approximate ranges for whole rock elemental compositions (XRF)*	TiO₂ (wt. %)	3.63–3.73	2.98–3.33	1.71–1.81	1.70–1.82
	MgO (wt. %)	3.25–3.90	1.9–3.1	3.8–4.9	4.9–5.5
	P₂O₅ (wt. %)	0.80–0.83	0.56–0.65	0.29–0.34	0.25–0.31
	Zr (ppm)	226–234	185–220	162–169	145–157
Magnetostratigraphy	Reverse	Normal	Normal (N2 MSU)	Normal (N2 MSU)	Normal (N2 MSU)
Notes	Crystal sizes for this unit are usually larger than underlying GRB units and are commonly in the range of 0.65–1.1 mm.	Crystal sizes for this unit are usually larger than underlying GRB units	Upper contact not well exposed	May be older than Spokane Falls member	Unit interfingers with an inflated Stember Creek member

*See text and *Data Supplement Table DS01* for more details. MSU: magnetostratigraphic units; mafic mineral abbreviations: cpx = clinopyroxene, ol = olivine, opx = orthopyroxene.

commonly aphyric, aphanitic (0.2–0.3 mm), where crystals are more commonly in the higher range of sizes (0.65–1.1 mm); euhedral; groundmass textures are mostly trachytic (somewhat oriented) and less commonly pilotaxitic (unoriented), and seriate texture is relatively common; autobreccias and entablatures are common, sometimes with well-developed platy flow foliation, but colonnades are not well-developed; see Table 2 for mafic mineral characteristics and elemental compositions (low Cr ~3–5 wt. %), and based on geochemical composition this unit is likely the basalt of Rosalia, a reverse polarity flow set within the lower Priest Rapids Member; unit thickness is approximately 300 ft, and contains at least one or two flows; unit is found in the southeastern corner of the map area at the northwestern extent of the Boylston Mountains, and exposures very likely continue to the southeast within and along these mountains; unconformably overlies the Vantage member (unit M_{CEV}). Reference localities include geochemistry sites G160 and G166 along Caribou Road.

M_{VWF} Frenchman Springs Member of Wanapum Basalt (Miocene)— Basalt; dark gray to grayish brown; well indurated; mostly microporphyritic, commonly coarse crystal sizes (0.75–1.2 mm), less commonly aphyric,

aphanitic; euhedral; groundmass textures are pilotaxitic (unoriented) and seriate; autobreccias and entablatures are common, sometimes with well-developed platy flow foliation, but colonnades are not well-developed; see Table 2 for mafic minerals and elemental compositions, and based on geochemical composition (elevated Cr 39–50 wt. %, and Nb >~14.5 ppm) this unit is likely the basalt of Sand Hollow, a normal polarity flow set within the upper Frenchman Springs Member; unit thickness is less than 200 ft, and contains at least one flow; unit is found in the southeastern corner of the map area at the northwestern extent of the Boylston Mountains, and exposures very likely continue to the southeast within and along these mountains; unconformably overlies the Vantage member (unit M_{CEV}). Reference localities include geochemistry sites G163 and G165 near Caribou Road.

M_{Vg} Grande Ronde Basalt (GRB), undivided (Miocene)— Basaltic andesite described in detail in the following units. GRB members are broadly mappable using a portable fluxgate magnetometer to place units into a magnetostratigraphic context. Previously mapped according to four polarity chronostratigraphic units or magnetostratigraphic units (MSU). From oldest to youngest: reverse magnetic polarity 1 (R1 MSU),

Table 2 continued. Main characteristics* of the units of the Columbia River Basalt Group (CRBG) in Colockum Pass SW and southern half of Naneum Canyon 7.5-minute quadrangles, northern Kittitas Valley.

Unit label		Mv _{gsmc}	Mv _{go}	Mv _{gg}	Mv _{gwr}	Mv _{gmh}
Unit thickness (ft)		150–200	300–500	600–900	> 400	> 200, base not exposed
Texture		aphyric, aphanitic	aphyric, aphanitic, diktytaxitic	aphyric, aphanitic	aphyric, aphanitic (to microporphyritic)	aphyric, aphanitic (to microporphyritic)
Crystal size (mm)		0.15–0.30, max 0.6 mm	0.2–0.6, max 0.9 mm	0.2–0.7	0.1–0.5, max 1.0 mm	0.25–0.55, max 1.75 mm
Mafic minerals (% , size, abundance)		20–30%	< 5%, 0.2 mm	20–25%, 0.3–1.0 mm, cpx>ol	5–30%, 0.1–0.8 mm	25–40%
Approximate ranges for whole rock elemental compositions (XRF)*	TiO ₂ (wt. %)	1.86–1.96	1.85–1.93	1.8–1.9	2.2–2.4	2.1–2.2
	MgO (wt. %)	4.2–4.9	3.4–3.7	3.9–4.2	3.2–3.6	3.9–4.1
	P ₂ O ₅ (wt. %)	0.28–0.30	0.30–0.32	0.29–0.33	0.42–0.50	0.38–0.43
	Zr (ppm)	156–160	185–196	162–173	194–201	168–174
Magnetostratigraphy		Normal (N2 MSU)	Normal (N2 MSU)	Reverse (R2 MSU)	Reverse (R2 MSU)	Reverse (R2 MSU)
Notes		P ₂ O ₅ as high as 0.37 wt.%, Zr as high as 170 ppm	Several thin flows are brownish orange stained (Fe-Ox). Unit is an invasive volcanic flow and contains peperitic hyaloclastite.	Thickness could be > 1,000 ft	More microporphyritic than other overlying members	Similar to Wapshilla Ridge in its abundance of microphenocrysts

*See text and *Data Supplement Table DS01* for more details. MSU: magnetostratigraphic units; mafic mineral abbreviations: cpx = clinopyroxene, ol = olivine, opx = orthopyroxene.

normal magnetic polarity 1 (N1 MSU), reverse magnetic polarity 2 (R2 MSU), and normal magnetic polarity 2 (N2 MSU) (Tabor and others, 1982; Reidel and Tolan, 2013; Hammond, 2013). Mapped GRB units are either N2 or R2 (Table 2). Unit Mv_g is mapped where geochemistry was unavailable, outcrops were lacking, inference for a subunit was overly speculative, or units were grouped at depth in cross section (for example, Grouse Creek (R2 MSU) and older units to R1 MSU).

Stratigraphy in our map area is remarkably similar to the stratigraphy of Hammond (2013) in the Naches River area and to the westward adjacent mapping by Sadowski and others (2020). Without the base exposed, total thickness of GRB rocks is poorly constrained. The thickness is inferred from geophysical modeling of gravity and aeromagnetic data, and may range from approximately 3,000–4,000 ft thick north of the Dead Coyote fault splays. Models of the geophysical data show thinner GRB in the range front and thicker GRB in the middle of Kittitas Valley (greater than 4,000 ft). CRBG thickness is interpreted from two hydrocarbon exploration boreholes east and southeast of the map area: Shell BISSA 1-29 well (API# 046-037-00006) and Meridian BN 23-35 well (API# 046-037-00009). These suggest thicknesses of ~4,600 ft and ~6,700 ft,

respectively (Wilson and others, 2008; Czajkowski and others, 2012), but do little to tightly constrain GRB thickness within the map area. With geophysical data modeling proposing thicker CRBG in the middle of Kittitas Valley, and these wells, particularly BN 23-35 being closer to the synclinal axis of the valley, we would expect available well data to show thicker CRBG overall. The northern map area is composed primarily of GRB with sedimentary interbeds. In general, thin sections show more euhedral than subhedral laths of plagioclase microlites intermeshed in an irregular, unoriented groundmass texture (textures that are pilotaxitic are more common than trachytic ones).

Mv_{gs} Sentinel Bluffs Member, undivided (Miocene)—Basaltic andesite; aphyric, aphanitic; the map area contains four subunits, from oldest to youngest: basalts of McCoy Canyon, Stember Creek, Spokane Falls, and Museum, where the middle two subunits are portions of the “Cohassett flow” (Reidel, 2005) that may be intermingling compositional types and may locally exhibit an internal vesicular zone (IVZ) related to “flow inflation” between the basalts of Spokane Falls and Stember Creek (McMillan

and others, 1989; Reidel, 2005). Where present, the IVZ may obscure the locations of vesicular flow tops identified via surface mapping of physical volcanology characteristics, because vesicular flow tops and the IVZ look similar. The Sentinel Bluffs Member is at least ~500 ft thick. The unit is thinnest at the range front, possibly as a result of uplift and erosion, and is likely thicker in synclines and in Kittitas Valley. The Sentinel Bluffs Member is commonly mapped along the northern margins of Kittitas Valley or along higher elevations in the northern map area. The unit was formerly mapped as GRB N2 MSU (Tabor and others, 1982). Unit **Mvg_s** is mapped where geochemistry was unavailable, but reasonable interpolations could be made using existing geochemical results (generally TiO₂: ~1.7–2.0 wt. %, MgO: ~3.8–5.5 wt. %, P₂O₅: ~0.26–0.36 wt. %, Zr: ~155–170 ppm); with available whole rock geochemistry, the Sentinel Bluffs Member is subdivided into:

Mvg_{sm} Basalt of Museum (Miocene)—Basaltic andesite; aphyric, mostly aphanitic commonly with medium crystal sizes (0.10–0.32 mm, as large as 0.55 mm); mostly entablature with rare, basal colonnade (geochemistry site G094); groundmass textures are pilotaxitic (unoriented) and seriate; see Table 2 for mafic minerals and elemental compositions; unit thickness is greater than 100 ft with upper contact not exposed, and may be thicker in synclines and in Kittitas basin; contains at least two flows; unit is widespread and found along lower portions of northern range front and at highest elevations toward Table Mountain; upper contacts with Vantage Member are possibly exposed in southeastern map area, but there are no outcrops to confirm GRB geochemistry there; reference localities include geochemistry sites G081, G082, G089, G094, G115, and G157. Note: the sample from geochemistry site G158 has a somewhat elevated loss on ignition percentage (LOI 2.80%). On a TiO₂-MgO variation diagram, this sample resides in the overlapping classification boundaries of basalt of Museum (unit **Mvg_{sm}**)

and the Grouse Creek member (unit **Mvgg**). It is possible that this sample is misclassified and may in fact have compositions more Grouse Creek-like than Museum-like, and if so, the fault geometries near Wilson Creek canyon may need to be reassessed.

Mvg_{ssc} Basalt of Stember Creek (Miocene)—Basaltic andesite; aphyric, mostly aphanitic with crystal sizes ranging from fine to coarse (0.1–0.5 mm, as large as 1.75 mm); common basal colonnade, interior entablature, and vesicular flow top; groundmass textures are pilotaxitic (unoriented) with equant microphenocrysts; elemental compositions (Table 2) of TiO₂ in weight percent are slightly lower than Spokane Falls, and elemental compositions of Zr in ppm are slightly lower than Spokane Falls; unit thickness is less than ~250 ft, may be thicker in Kittitas basin, and thins eastward (~70 ft thick on Cross Section A–A') and may pinch out; contains at least two flows; consistently overlies Spokane Falls-type compositions, but may instead interfinger with the Spokane Falls-compositional type (see eruptive sequence of Cohasset Flow in figure 5 of Reidel, 2015 and details in Reidel, 2005); unit is well exposed on the east side of Naneum Canyon, at middle and higher elevations, and is as common as the basalt of Spokane Falls; reference locality includes geochemistry site G037.

Mvg_{ssf} Basalt of Spokane Falls (Miocene)—Basaltic andesite; aphyric, mostly aphanitic with crystal sizes ranging from fine to medium (0.07–0.55 mm); common basal colonnade, interior entablature, and vesicular flow top; groundmass textures are pilotaxitic (unoriented) with equant microphenocrysts; elemental compositions (Table 2) of TiO₂ in weight percent are slightly higher than Stember Creek and

of Zr in ppm are slightly higher than Stember Creek; unit thickness at least ~250 ft and may be thicker in synclines and in Kittitas basin, may pinch out northward, and, notably, unit thickness in the BISSA well farther east is ~640 ft (S. Reidel, WSU Tri-Cities, written commun., 2020); contains one to three flows and thin, irregular hyaloclastite horizons, particularly near its base and middle, and contains thin sedimentary interbeds; consistently underlies Stember Creek-type compositions (possibly near IVZ), but may instead interfinger with Stember Creek-type compositions (see eruptive sequence of Cohasset Flow in figure 5 of Reidel, 2015 and details in Reidel, 2005); found commonly in northern range front and middle elevations; upper and lower contacts generally inferred using changes in physical volcanology paired with geochemical results; iron-oxide(?)—filled vesicles at geochemistry site G117; reference localities include outcrops along Cooke Canyon Road and geochemistry site G155.

Mv_{gsmc} Basalt of McCoy Canyon (Miocene)—Basaltic andesite; aphyric, mostly aphanitic commonly with medium crystal sizes (~0.15–0.30 mm, as large as 0.6 mm); forms well-developed entablature with short basal colonnade and common vesicular flow top; groundmass texture is pilotaxitic (unoriented); see Table 2 for elemental compositions; unit thickness is ~150–200 ft and may be thicker in synclines and in Kittitas basin; contains at least two flows and thin hyaloclastites are usually at unit's base and near its upper contact with unit Mv_{gssf}; commonly overlies the Coleman member of the Ellensburg Formation (unit Mc_{ec}); reference localities include geochemistry sites G012, G065, G132, and G133.

Mv_{go} Ortley member—Basaltic andesite; aphyric, mostly aphanitic, commonly with medium crystal sizes (0.2–0.6 mm, as large as

0.9 mm); well-developed vesicular flow tops with brownish orange-stained (iron-oxide) exposures are very common. These thin (<20 ft) flow tops can be easily traced from a distance in Coleman Canyon. These flow tops contain well-developed flow foliations. Basal colonnades and interior entablatures are thin, poorly developed, and may even look similar to each other. Groundmass texture is pilotaxitic (unoriented), weakly microporphyritic, and mildly microvesicular (diktytaxitic). Mafic minerals (Table 2) are less common in this unit than in other GRB members. Elemental compositions (Table 2) are similar to the underlying Grouse Creek member, TiO₂ weight percents are slightly higher than Grouse Creek, and MgO weight percents are slightly lower than Grouse Creek. WSU's ML model returned low confidence classifications for nearly all samples of the unit. Stratigraphic relationships and geochemical variation diagrams (TiO₂ vs. MgO and TiO₂ vs. P₂O₅) from Hammond (2013) and Sadowski and others (2020) aided unit classification. Unit thickness is ~300–500 ft, and may be thicker in synclines and in Kittitas basin. Unit is common in the middle elevations of deep canyons, lower elevations of shallow canyons, and in the cores of monoclines. Unit includes at least three flows. The Ortley member has a well exposed bottom contact with the Grouse Creek member (unit Mv_{gg}) at age site GD01, and has an upper contact with the sedimentary Coleman member (unit Mc_{ec}). Unit was likely eroded followed by the deposition of the Coleman member. The Ortley member also conformably overlies the Grouse Creek member (unit Mv_{gg}), and magnetic polarity typically distinguishes these units apart (Reidel and Tolan, 2013), where Ortley is near the base of the N2 MSU and Grouse Creek is near the top of the R2 MSU. Abundant hyaloclastite and pillow breccia are common at the contact between these two units. Siltstone (age site GD01) enveloped by pillow breccia within this unit near its base strongly suggests that portions of the Ortley member are locally invasive and contain peperitic hyaloclastite (peperite). Sadowski and others (2020) may have under-mapped the Ortley member in the westward adjacent quadrangles because of lack of geochemical and magnetometric data, and there is very likely more Ortley member—and less Grouse Creek member—than previously recognized to the west (See scratch boundary on western map boundary). Reference localities include

geochemistry sites G015, G054–G056, and G096.

Mv_{gg}

Grouse Creek member (Miocene)—Basaltic andesite; aphyric, mostly aphanitic with crystal sizes ranging from medium to coarse (0.2–0.7 mm, typically >0.5 mm); mostly fanning entablatures, rarely platy, where colonnades and vesicular tops are thin, poorly developed to absent in the unit's interior; commonly contains hyaloclastite with or without peperite; groundmass texture is pilotaxitic (unoriented) and groundmass crystal sizes are slightly greater than those of unit **Mv_{gs}**; elemental compositions (Table 2) of TiO₂ in weight percents are slightly lower than the Ortley member and of MgO in weight percents are slightly higher than the Ortley member; WSU's ML model returned low confidence classifications for nearly all samples of the unit. Stratigraphic relationships and geochemical variation diagrams (TiO₂ vs. MgO and TiO₂ vs. P₂O₅) from Hammond (2013) and Sadowski and others (2020) aided unit classification. Note: geochemical data from Hammond (2013) and Sadowski and others (2020) were not included in the geochemical training set for the ML model. Therefore, insufficient training of the ML model may be responsible for the low confidence classifications of the geochemistry results for unit **Mv_{gg}**. Unit thickness is 600–900 ft and may be thicker (>1,000 ft). The unit breaks into two thick fanning entablatures that exhibit at least two flows and probably more (less than six?). Unit spans low to mid elevations in deep canyons (Coleman and Naneum). Unit is commonly associated with hyaloclastite, especially at the contact with the Ortley member (unit **Mv_{go}**) and deep in Coleman Canyon, suggesting that portions may be invasive, similar to the Ortley member. Unit was previously mapped as the Howard Creek invasive flow by Rosenmeier (1968) and (or) GRB R2 MSU by Tabor and others (1982). Sadowski and others (2020) may have over-mapped the Grouse Creek member in the westward adjacent quadrangles because of lack of geochemical and magnetometric data, and there is very likely more Ortley member—and less Grouse Creek member—than previously recognized to the west (See scratch boundary on western map boundary). Reference localities include geochemistry sites G046 and G053.

Mv_{gwr}

Wapshilla Ridge Member (Miocene)—

Basaltic andesite; aphyric, mostly aphanitic to microporphyritic with crystal sizes ranging from medium to coarse (0.1–0.5 mm, rarely >1.0 mm) including minor phenocrysts of plagioclase; contains well-developed basal colonnades and vesicular tops and common entablatures; groundmass texture is pilotaxitic (unoriented) and microporphyritic or otherwise seriate; mafic mineral percentages (Table 2) are slightly lower than Mount Horrible; elemental compositions (Table 2) are similar to the underlying Mount Horrible member with P₂O₅ weight percents slightly higher than Mount Horrible and Zr ppm slightly higher than Mount Horrible; unit thickness is at least ~400 ft and is likely thicker; contains at least two exposed flows; best exposed at lower to middle elevations in Naneum Canyon, where base is exposed above unit **Mv_{gmh}**; fragments of petrified wood are common near an exposure about one-third up the east side of Naneum Canyon (significant site S02); reference localities include geochemistry sites G150 and G025.

Mv_{gmh}

Mount Horrible member (Miocene)—

Basaltic andesite; aphyric, mostly aphanitic to microporphyritic with crystal sizes ranging from medium to coarse (0.25–0.55 mm, as large as 1.75 mm, slightly coarser than Wapshilla Ridge) including minor phenocrysts of plagioclase; groundmass texture is pilotaxitic (unoriented) and microporphyritic; mafic mineral percentages (Table 2) are slightly higher than Wapshilla Ridge; elemental compositions (Table 2) are similar to overlying Wapshilla Ridge member, where P₂O₅ weight percents are slightly lower than Wapshilla Ridge and Zr ppm are slightly lower than Wapshilla Ridge; unit thickness is likely greater than 150 ft, but the base is not exposed; contains at least one or two flows; exposed in the deepest portions of Naneum Canyon; the upper contact with Wapshilla Ridge member is generally subtle and also geochemically gradational with unit **Mv_{gwr}** (geochemistry site G149). Reference localities include geochemistry site G022.

Pre-Miocene Bedrock

ØEc

Continental Sedimentary Rocks, undivided (Oligocene to Eocene)(cross section only)—Unit

may include tuffaceous siltstone and sandstone of the Oligocene to Eocene Ohanapecosh Formation, coaliferous sandstone, tuffaceous(?) siltstone, minor rhyolite of the Eocene Roslyn Formation, and (or) sandstone and conglomerate of the Eocene Swauk Formation.

Unit combines sedimentary units above and below the Eocene Teanaway Formation.

LITHOLOGIES DEPICTED AS OVERLAYS

Mass Wasting (overlay mw)

These are areas where landforms suggest mass movement on unstable slopes, but evidence for landslide deposits is inconclusive. Overlays encompass hummocky or irregular ground surface patterns but boundaries of overlays generally lack unambiguous head scarps, lateral head scarps, or toes that units Qls or Qlso otherwise exhibit. Mass wasting overlays are usually at higher elevations and may indicate areas of solifluction, which are gradual downslope mass movements related to freeze-thaw cycles.

Quaternary Loess (overlay Ql)

Loess is light brown to medium brown, moderately weathered; low density, poorly compacted; composed of silt to very fine grained sand; angular; moderate to poor sorting, matrix-supported; internally structureless forming 3-foot-tall, irregularly spaced mounds with varying amounts of post-depositional fluvial dissection; windblown loess is widespread and most commonly blankets older alluvial deposits (units QRcg, Qaf4, and Qaf3) in the central to northern map area. There are also patchy mounds of loess on bedrock surfaces (subunits of Mvgs) at higher elevations between Naneum and Coleman Canyons in the northern map area. Deposits are found on flat to gently sloping surfaces where they cover units of various ages and elevations. Locally, loess mounds are also called patterned ground or Manastash Mounds. We agree with the interpretation that their origins are the result of intensive frost action under a periglacial climate (Kaatz, 1959; Williams and Masson, 1949); anastomosing surface textures with ~1–3 ft deep incisions that are ~2–15 ft wide suggest that fluvial incision and erosion may also aid generation or modification of these mound landforms. This deposit correlates with the eolian loess of the Palouse Formation, found throughout eastern Washington. Age is approximately Holocene to Late Pleistocene.

Miocene Hyaloclastite (overlay hy)

Hyaloclastite is a volcanoclastic aggregate consisting of pillow breccia with volcanic glass and its weathered counterpart palagonite, and is in some places peperitic; light yellowish brown to orange brown or tan, strongly weathered; moderate density, moderately well-consolidated; generally sand to boulder grain sized with a very fine grained matrix; angular to subangular; poorly sorted, matrix-supported; generally convoluted and structureless, and exposures may contain basalt pillows that are matrix-supported or have fragments of breccia; less commonly pillow-supported (see roadcuts north and south of age site GD01); centimeter- to meter-scale pillow fragments have chilled margins and radial interior jointing akin to entablature; vesicles can be common in the basaltic material and collectively form pillow, palagonite, vesicular complexes (PPVC); clastic aggregates characteristically include basaltic glass (tachylite ± sideromelane), palagonite, and plagioclase crystals; thickness varies from several feet up to about 150 ft; unit is associated with many basaltic and sedimentary exposures and is most commonly

found near the contact between the Grouse Creek and Ortleay members (units Mv_{gg} and Mv_{go}) and between the lower basalts of the Sentinel Bluffs Member (in unit Mv_{gsmc} and especially in unit Mv_{gssf}). These field relationships support locations of paleotopographic low elevations preceding and after the depositional time of the Coleman member (unit MC_{ec}). Exposures of hyaloclastite decrease northeastward toward Cooke Canyon. These lithologic characteristics and spatial associations suggest that the hyaloclastite was locally generated from quenching with consequent fracturing, disintegration, and weathering of GRB lavas as they entered a Miocene water body. Siltstone at age site GD01 is encapsulated by palagonite and large (1 m-scale) pillow breccia fragments, and suggests that portions of unit Mv_{go} may be an invasive basalt flow or peperite, as previously suggested by other authors (Rosenmeier, 1968; Tabor and others, 1982). Peperitic hyaloclastite is not as common as pillow breccia and PPVC, which lack a sedimentary component. Age is presumed to be similar to the Miocene basalts they reside in. Reference localities for hyaloclastite include geochemistry site G079 and age site GD01.

DISCUSSION OF GEOLOGIC STRUCTURES

This year's mapping identifies, characterizes, and refines the locations of geologic structures, including reverse faults, oblique faults, and several types of folds. Most of these structures were first identified by Bentley (1977), Waitt (1979), and Tabor and others (1982). These previously identified faults and folds include: the Dead Coyote fault (DCF), Dry Creek fault (DrCF), Craigs Hill fault (CHF), and Wilson Creek and Reecer Canyon monoclines (WCM and RCM, respectively). All of these were recently mapped in the westward adjacent quadrangles (Ellensburg North and Reecer Canyon) by Sadowski and others (2020). The sections below discuss these geologic structures in more detail, including their associated geophysical anomalies. Figure 1 summarizes the structures well supported by geological data, whereas structural features discussed that are not on Figure 1 are supported by geophysical anomaly gridding and modeling of aeromagnetic and gravity data.

West-Striking Faults

Previously mapped west-striking faults of Sadowski and others (2020) that project into this year's map area—the DCF, DrCF, and CHF—have geometries refined by recent mapping. West-striking faults are generally reverse and predominantly dip-slip, possibly with some oblique motion, and are likely high-angle near the surface. It is unclear if these faults dip more gently at depth (listric?).

The north-dipping DCF splays into two diverging fault strands—a southern and northern splay—east of where they were mapped as subparallel by Sadowski and others (2020) (labels DCFs and DCFn, respectively on Fig. 1). The southern strand continues eastward to link with a long, northwest-striking range front fault (label NWF on Fig. 1). It isn't clear how far east the northern strand continues, but it may also link up with the same northwest-striking range front fault. The southern splay of the DCF produces a prominent escarpment on Quaternary deposits

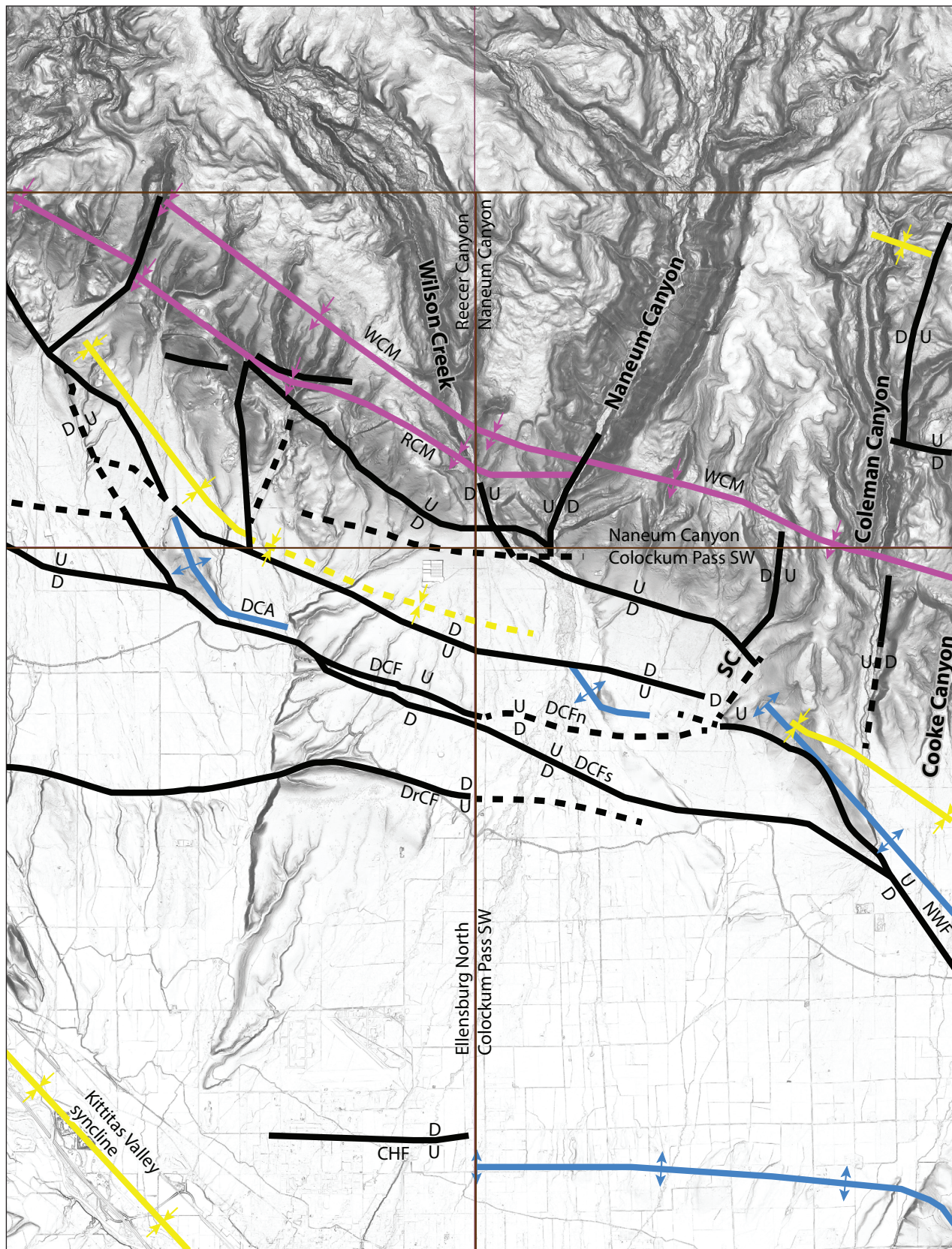


Figure 1. Reference map showing only the geologic interpretations of structures in northern Kittitas Valley from this year's mapping and Sadowski and others (2020). Map key: faults are black and dashed where questionable; anticlines are blue, monoclines are pink, synclines are yellow, U/D mean upthrown/downthrown fault blocks. Possible hard-linked fault step-over is dashed and east of the SC label that is located at the mouth of Schebly Canyon.

Acronyms: CHF, Craigs Hill fault; DCF, Dead Coyote fault; DCFs, southern splay of the Dead Coyote fault; DCFn, northern splay of the Dead Coyote fault; DrCF, Dry Creek fault; NWF, unnamed northwest-striking range front fault; RCM, Reecer Canyon monocline; SC, Schnebly Canyon; WCM, Wilson Creek monocline; DCA, Dead Coyote anticline.

(unit Qaf3) in the central map area west of Cross Section A–A'. No fault surfaces related to these faults were found in the map area.

The DCF is evident in the geophysics and has the best placement and constraint on its location of all the faults modeled (Fig. M1B). The DCF has a distinctive east-trending gravity gradient and linear low aeromagnetic anomaly (DCF and DCA in Fig. M1A). The aeromagnetic low related to the DCF continues eastward from the Reecer Canyon quadrangle, where it originates from a fault-related anticline in the hanging wall (Sadowski and others, 2020), and links with an unnamed, northwest-striking range front fault. The dip of the DCF ($\sim 70^\circ$ N, Fig. M1B) is constrained by geophysical modeling, where the only geologically feasible model includes: (1) matching the tip of the fault in the model with the mapped location of its surface trace, and (2) precise positioning of the required offsets in the GRB along the trace at depth to match gravity and magnetic anomalies across the fault. The DCF has well-constrained displacements from the geophysical anomalies because it breaks the top of the CRBG package and creates a short-wavelength gravity gradient there (Fig. M1B). Other fault displacement magnitudes are not as well constrained because uncertainties in unit physical properties produce uncertainties in modeled unit thicknesses within the CRBG.

The Dry Creek fault (DrCF) and Craigs Hill fault (CHF) have poor geologic evidence at the surface in this year's map area relative to the Ellensburg North and Reecer Canyon quadrangles mapped in 2020. These faults lack fault scarps and fault surfaces. We now consider that the geomorphic evidence of uplifted alluvial landforms associated with these two "faults" may be better attributed to folding in the shallow subsurface within this year's map area rather than faulting. This does not preclude a relationship to concealed faulting at depth, but merely that we lack the geological evidence at the surface to firmly support a fault on the geologic map in this year's map area. Whereas geophysical modeling supports the existence of the DrCF (Sadowski and others, 2020), the modeling is not as conclusive for the CHF. Geophysical anomalies for the CHF are ambiguous and show a subtle east–west trending gradient in the southwestern part of the Colockum Pass SW quadrangle, which could result from folding alone (CHF in Fig. M1A). If the CHF exists in the Colockum Pass SW map area, there likely is a genetic relationship between it and the anticline to the south.

Northwest-Striking Faults

Northwest-striking faults are generally inferred to be dextral(?)–reverse given the ~ 16 Ma-to-modern stress regime of clockwise rotation and compression (Wells and McCaffrey, 2013). A long, unnamed fault produces northwest-trending escarpments along the range front and is likely responsible for the bedrock rise and elongate hillcrest that protrudes southward into Kittitas Valley to the south–southwest of Coleman Canyon (label NWF in Fig. 1). Northwest of these escarpments and west of Schnebly Canyon, a ~ 25 -ft-tall fault surface is exposed in a basalt quarry (geochemistry site G138), the only fault surface found in the map area. The fault surface exhibits subhorizontal slickenlines on a subvertical surface that has subhorizontal corrugations, where troughs are parallel to the slickenlines. These observations on a northwest-striking fault suggest mostly strike-slip displacement

on northwest-striking structures. Accordingly, we infer that the well-located fault in the range front between Schnebly and Coleman Canyons also exhibits a considerable proportion of strike-slip displacement.

Geophysically, the unnamed northwest-striking range front fault (NWF on Fig. 1) has a distinctive, southeast-trending gravity gradient and a linear, low aeromagnetic anomaly (NWUF and NWA1 in Fig. M1A). This aeromagnetic low links with the DCA's low aeromagnetic anomaly near the unnamed fault's escarpments and continues southeast into the adjacent Colockum Pass SE quadrangle. The linking of the DCF and northwest-striking faults is supported by the linking of their respective associated geophysical anomalies (Fig. 2). This suggests that these faults are kinematically connected through this region. The northwest-trending magnetic low itself was difficult to interpret and model with fold-thrust style geometries, giving us confidence in our preferred solution, which suggests a geologic history of reactivated faults (Fig. M1B). This solution suggests structural inversion whereby the original northwest-striking transtensive fault—active during Wapshilla Ridge and Grouse Creek member eruptions—was later reactivated as a reverse fault. Transtensive faulting allowed accumulation of thicker packages of basalts with strong reversed magnetic remanence. Later reverse faulting uplifted these reversed members toward the surface and folded them, thus creating the linear magnetic anomaly we observe (see the *Blind Transtensional Faults* section below for further discussion of the earlier history).

Northerly Striking Faults

The northward continuation of north–northwest through north–northeast striking faults is uncertain based on geologic evidence alone. Offset GRB stratigraphy is observed near the mouths of Wilson, Naneum, and Schnebly creeks and the northern reaches of Coleman Canyon, but northerly striking faults are not well exposed. Where observed, their senses of slip are not clear. They are inferred to be high angle, and given the regional stress regime of ongoing north–south compression, northerly striking faults are tentatively inferred to exhibit oblique strike-slip motion (wrench faulting?) with some unknown proportion of dip-slip motion. We did not observe escarpments related to northerly striking faults in Quaternary deposits and these faults are suggested primarily by geomorphological evidence: straight, narrow, and deep canyons where we suspect these faults are concealed. We are careful not to rely on "straight canyons" alone to support our fault interpretations, and consider geologic, geomorphic, and geophysical evidence.

Upstream to the north, there appear to be small elevation changes in GRB stratigraphy across the canyons, which could support the presence of faults. However:

1. Geologic contacts are not always accurately located and changes in contact elevation may result from uncertainty related to mapping of approximately located or inferred contacts, and not faulting,
2. Apparent changes in GRB dip may be related to lava flow anisotropy or irregular cooling textures instead of tectonic deformation,

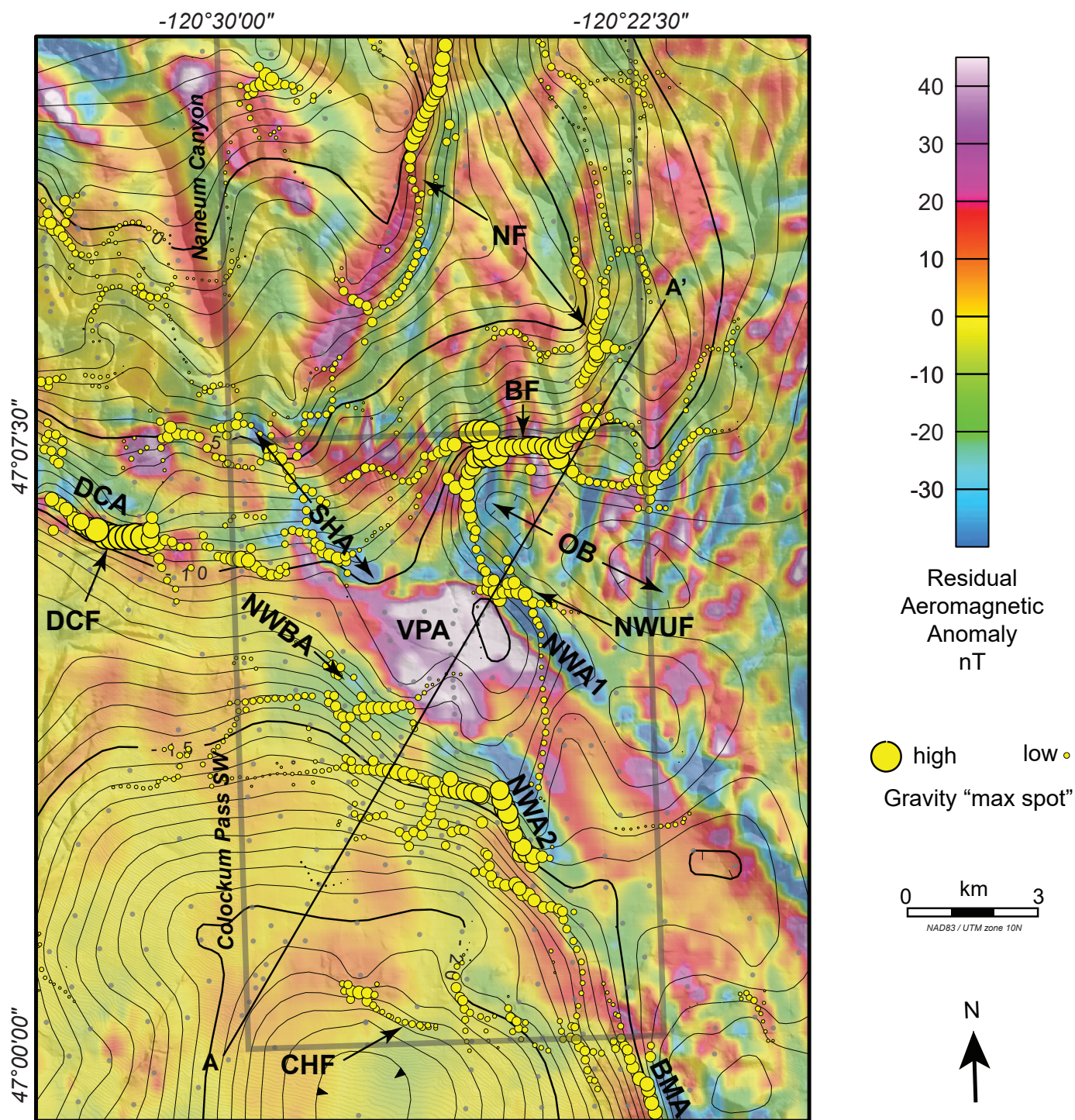


Figure 2. Geophysical interpretation for the map area with filtered data that shows combined isostatic gravity and residual aeromagnetic data. Gravity contours are 0.5 mGal and hachures indicate closed lows. Hillshade topography helps provide orientation in the background. Gravity stations are gray dots. Relative size of the gravity max spots are proportional to the magnitude of the gravity gradient in that location. The residual aeromagnetic map results from subtracting a version of the original aeromagnetic grid that has been filtered (upward continued 50 m) to enhance long-wavelength anomalies from the original grid. The remaining residual retains short-wavelength anomalies that mainly reflect the effects from shallow sources (upper few kilometers). This method does not produce anomalies reflecting a precise depth of sources, but can separate out anomalies sourced from generally deeper or generally shallower sources. In particular, this method enhances linear, low magnetic anomalies interpreted to be from long-hinged anticlines in the region (for example DCA, NWA1, NWA2, NWBA).

Geophysical feature acronyms discussed: BF—Blind faults; BMA—Boylston Mountain anticline; CHF—Craigs Hill fault gradient; DCA—Dead Coyote anticline; DCF—Dead Coyote fault; NF—north-striking faults; NWA1—northwest-trending long-hinged anticline #1; NWA2—northwest-trending long-hinged anticline #2; NWBA—northwest-trending broad anticline; NWUF—northwest-trending unnamed fault; OB—Older basin gravity low; SHA—Short-hinged anticlines; VPA—volcanic pipe aeromagnetic high.

3. Flat lying stratigraphy make it difficult to detect any component of strike-slip displacement, or
4. The straight canyons may instead represent relict bedrock fractures, jointing, diking, or conjugate structures (for example, Riedel shears: J. Powell, DNR, oral commun., 2021) that lack displacement, which the creeks exploited.

We more closely examine the geomorphology of Naneum Canyon and Wilson Creek. Qualitative analysis of the lengths of tributaries to Naneum Creek on each side of Naneum Canyon show that tributaries on the westside are longer than those on the eastside. This geomorphological evidence shows drainage basin asymmetry and there are many possible explanations for that, one of which is differential uplift or tilting with east-side down motion. An anomalous alluvial fan surface near the mouth of Wilson Creek (unit Qaf2 at significant site S01) may be affected by faulting. Despite the creek incising through it, this fan surface (strath terrace?) is smoother and more elevated than its adjacent active alluvium (unit Qa) to the north and south. These differences in morphology and elevation over a short distance suggest that this area may have been uplifted.

Geophysical anomalies for these northerly-striking faults are challenging to interpret. Magnetic anomalies trend up the deep canyons these creeks are in, but these magnetic anomalies may be from topography exposing layered basalts with different physical properties. More revealing are gravity gradients, which also trend parallel to the deep canyons (NF in Figure M1A), and unequivocally show lower gravity to the east. Lower gravity commonly results from lower density rocks. The nearby Swauk and Roslyn Formations are lower density sedimentary rocks that were deposited in transtensional Eocene basins bounded by northerly striking faults. Therefore, we suspect that the north trending gravity gradients may be northerly striking, pre-CRBG structures that bound areas with lower density sedimentary rocks to the east along which straight canyons have developed. It is reasonable to infer that possible pre-CRBG structures are related to post-CRBG deformation in these canyons. If these two things are related, then it suggests post-CRBG re-activation of pre-existing faults. How these deeper inferred structures project to the surface is unclear at present.

Bend in Range Front

A prominent bend in the range front near Schnebly Canyon (label SC in Figure 1) marks the transition from west-striking structures to northwest-striking structures. At this bend, strain transfer may have occurred—or is occurring—among west-striking and northwest-striking faults, which produced this area of structural complexity. More specifically, these faults are the aforementioned linked fault splays of the DCF and unnamed northwest-striking fault(s) (NWF label on Figure 1). Strain may have also transferred among the range front faults themselves, including the NWF. Near the mouth of Schnebly Canyon, there is also a hard-linked(?) fault step-over where the NWF steps to the right and north toward the range front fault (Figure 1, hard-linkage(?) is northeast striking, dashed, and east of the SC label).

Also notable in this bend is a rounded, high aeromagnetic anomaly that obscures the linkage between these west-trending and northwest-trending aeromagnetic anomalies (VPA in

Figure M1A). The low aeromagnetic anomaly associated with the DCF also produces a local disturbance in this otherwise very strong aeromagnetic high (Figure 2, relative low of pink surrounded by white directly under the VPA label). It may not be a coincidence that this strong magnetic high is in this area of structural complexity. A deep block of magnetic material, the top of which must extend at least to the depth of the base of the CRBG, is responsible for this anomaly. In addition, it must be narrow with steep sides (Figure M1B). The physical parameters—density ($2,720 \text{ kg/m}^3$) and magnetic susceptibility ($135 \times 10^{-3} \text{ SI}$)—combined with the steep-sided geometry suggest a mafic intrusion such as diorite, basalt, or diabase in a volcanic pipe. The pipe's location at this area of structural complexity may have genetic implications for the pipe or the faults. Maybe the intrusion took advantage of the crustal weakness created by the faults at this bend to intrude there, or the faults took advantage of the intrusion's rheologic influence to initiate here. Granted, we know the faults here are Miocene and younger, and can only speculate that they also have a prior history. The exact age of the mafic intrusion is unknown and we speculate that it could be Miocene or older.

Blind Transtensional Faults

Blind faults are inferred from gravity and aeromagnetic anomalies and from forward modeling of these geophysical data. They do not have geologic evidence at the surface and are therefore delineated on the map using geophysical lineaments. Interpreted blind faults (Figure M1B) strike west and northwest and must dip very steeply in the near surface to fit steep, short-wavelength gravity gradients shown by the data. They may be related to concealed folds that are also inferred from the geophysical modeling.

One of the most conspicuous details of the gravity map is the large gravity low within the mountain front in the northeastern part of the Colockum Pass SW quadrangle (OB in Figure M1A). It is especially unusual given the lack of remarkable structures found by recent and previous geologic mapping. The gradients on the edges of the gravity low are very steep (BF and NWUF in Figure M1A), and such a short wavelength cannot be modeled with deeper basement structures nor with topography on the bottom of the CRBG, both of which produce long wavelength anomalies. So, these gravity gradients must be due to blind faults within the CRBG. To explain a large gravity low from a zone within the CRBG requires rocks with lower density than basalt. There are two logical possibilities: thicker packages of sedimentary rocks ($\sim 1,600\text{--}1,900 \text{ kg/m}^3$) or hyaloclastite ($\sim 2,200 \text{ kg/m}^3$) interbedded with the basalt.

Closer inspection of the aeromagnetic data shows a subtler, broad aeromagnetic low collocated with the gravity low (see values $<250 \text{ nT}$ collocated with OB in Figure M1A). In our modeling, the only geometry that can explain this low is a wedge of thicker rock with strong, reversed remanence in the subsurface. This broad low can't simply be due to a wide anticline, since our combined geological cross section interpretation and geophysical modeling don't support reversed units (such as the Wapshilla Ridge or Grouse Creek members) close enough to the surface to fit the aeromagnetic low. These reversed units could be thickened by reverse-to-thrust faults (strata duplicated by faulting) active after the eruption of the GRB, but one would need duplexing at

depth. However, duplexing would generate more near-surface folding than is observed in the geologic mapping.

The southern edge of the gravity low is bound by the unnamed northwest-striking fault and its associated linear magnetic low (NWUF and NWA1 in Fig. M1A). Along the northern edge of the gravity low, a west-trending gravity gradient (BF in Fig. M1A) with a stepping profile (best viewed in Fig. M1B) is not easily attributable to a mapped geologic structure, and does not exhibit the telltale pattern of a linear magnetic low indicating a hanging wall anticline within a reverse fault. Therefore we interpret south-dipping faults here. The coincidence of the need for (1) thicker basalts with strong reversed remanence, and (2) abundant low density material at a depth within the CRBG collectively suggest a transtensive, pull-apart basin with multiple bounding faults (Fig. M1B), accommodating the thicker basalts and sediments. Some of the bounding faults are blind and probably inactive, and some (like the unnamed northwest-striking fault) have been reactivated as reverse-oblique structures. Geometries of blind faults are simplified as planar in the cross section and geophysical model (Fig. M1B) and may be related to older strike-slip, transtensive tectonics. It is possible that these blind faults may exhibit more complicated geometries (for example, curved with transtensional, fault-related folds, or blind fold-thrust belt styles of deformation). We do not have geologic data to fully support or refute the sub-basin geometries we propose. We find the general ideas in our geophysical model plausible: where an older sub-basin, bound by old faults, was buried by younger flows.

Folds

Monoclines and anticlines are the most common folds in the map area. Synclines are less commonly observed. A laterally extensive, long-hinged monocline is located to the north of the range front. Anticlines of various geometries are near the range front and in the valley.

MONOCLINES

The Wilson Creek and Reece Canyon monoclines (Tabor and others, 1982; Sadowski and others, 2020) nearly intersect near Naneum Canyon in the western portion of the map area (labels WCM and RCM, respectively, on Fig. 1). We infer that only the Wilson Creek monocline continues farther east to the eastern map boundary. Monoclinal folding is progressively less pronounced eastward in the map area, and therefore more homoclinal between Cooke and Coleman canyons along Cross Section A–A'. Map patterns suggest that the monocline may also plunge east. This eastward plunging may also explain the differences in elevations of GRB contacts across northern Naneum Canyon.

ANTICLINES AND SYNCLINES

Long-hinged and short-hinged anticlines are well located with surficial mapping and geophysical data in the central and southeastern portions of the map area. We infer that these are fault-related folds. In all places in Kittitas Valley where we have geophysical modeling of the subsurface, narrow, linear magnetic lows correspond with basalt that has strongly reversed remanence closer to the surface at the apex of an anticline. Therefore we use this association to inform where we map anticlines.

In addition to the extensive anticlines associated with the northwest-striking fault discussed above, another long-hinged, northwest-trending anticline is mapped at the northwestern tip of the Boylston Mountains in the southeast corner of the map area. The anticline takes an acute bend to the west before trending along a series of low hills of unit QRcg. Notably, different dip values on units of different ages on the southern limb of this anticline record a history of tilting with calculable rates of deformation. In the southeast map area, there is an angular unconformity between units Mvwp (geochemistry site G160) and Mce (age site GD03) across which there is 10 degrees of discordance. The difference in age between the two units is approximately 9 Ma, resulting in a time-averaged tilting rate of ~1 degree per million years. The unconformity itself is also tilted and covered by Quaternary sediment, implying that there has been 20 degrees of tilting since 5.7 Ma at a time-averaged rate of ~3.5 degrees per million years. Although the two rates appear to indicate an increase in tilting through time, we are unsure if this is true because we do not have good temporal resolution between 5.7 and 15 Ma.

As discussed above, it is possible that this fold is related to a blind fault at depth—the Craigs Hill fault (Tabor and others, 1982; Sadowski and others, 2020), or related to faulting on the southwest flank of the Boylston Mountains. A linear, aeromagnetic low is collocated with the Boylston Mountains anticline (BMA in Figure M1A). This low continues approximately on trend with the anticline almost all the way to the DCF with a couple of very small right steps along the way (NWA2 in Figure M1A), suggesting continued anticlinal deformation to the north-northwest. We don't have a geological interpretation here because the area is concealed by Quaternary deposits, but the aeromagnetic anomaly strongly supports a concealed anticline making this northwest-trending anticline long and continuous. Just southwest of the DCF, this linear aeromagnetic low steps to the west (NWBA in Figure M1A), and we model a broad anticline at this location in our geophysical model (Figure M1B).

Short-hinged anticlines are located throughout areas immediately south of the range front and are identified by hills composed of volcanic bedrock or older alluvial fans. These folds are where the range front bends, and it is unclear if these short-hinged anticlines were connected or not. A continuous anticline may have been dissected and offset by the DCF fault splays, or these short-hinged anticlines may be doubly-plunging. Aeromagnetic anomalies support the fault-anticline complexity in this region with short, linear magnetic lows abruptly ending, coincident with mapped fault locations (SHA in Figure M1A). The trend of two of the magnetic lows northwest of the pipe (VPA in Figure M1A) broadly align with the long-hinged magnetic low northwest of the Boylston Mountains anticline (NWA2 in Figure M1A). Therefore, not all strain associated with this structure is completely transferred to the west-striking fault system.

Synclines are less common and somewhat questionable in the map area. There is a subtle syncline near the eastern range front that may project farther southeast to the adjacent quadrangle. There is another syncline that was observed on the west-facing cliffs of Coleman Canyon in the northeast corner of the map area. It is unclear if these two synclines are tectonic or may instead be related to the eruption and irregular emplacement

of Miocene lavas (in other words, cooling features). Conversely, in the map area anticlines have smaller interlimb angles and are less subtle than synclines, therefore we more readily attribute anticlines to tectonism (not cooling features).

WATER RESOURCES IN THE COLEMAN MEMBER

Hydrogeologically, the Coleman member is inferred to be a confined sedimentary aquifer with water resource potential. Its medium grain size, mild cementation, considerable thickness, and lateral extent are favorable characteristics for a productive water resource. It generally dips basinward from the uplands of the Okanogan–Wenatchee National Forest—its potential recharge area via precipitation—and very likely flattens out in the subsurface beneath Kittitas Valley. In the valley it exhibits the classic architectural characteristics of a confined aquifer with possible artesian flow, if penetrated. This classic textbook notion and its intrinsic properties of porosity and permeability need to be evaluated in more detail before development as a water resource. It may be at an economically accessible depth to the north of the DCF fault, but it isn't clear if this reverse fault serves as a permeability pathway or a seal that compartmentalizes the reservoir to the north. We suspect that, given the compressional state of regional stress, this fault is a barrier—or at least a baffle—to flow and compartmentalizes the Coleman member between it and the range front.

RECOMMENDATIONS FOR FUTURE RESEARCH

- Assess fault scarps in Quaternary and Tertiary deposits. Escarpments related to the range front fault southwest of Coleman Canyon and the southern splay of the DCF should be evaluated in more detail to assess their age, recency of activity, and offset using ground penetrating radar (GPR), paleoseismic trenching, and more detailed surficial mapping of alluvial and colluvial deposits.
- Transverse geophysical modeling. Forward modeling of additional high-resolution, closely-spaced gravity data collected in Naneum Canyon and collected transversely west-to-east from Wilson Creek to Cooke Canyon may elucidate complex structural and pre-Miocene basin architectural characteristics. Research challenges include the steep topography of the west–east traverse and the extreme terrain corrections needed for the gravity data.
- Assess subsurface reservoir conditions for the Coleman member. Drilling into the Coleman member near the range front will support hydrogeological and hydrological investigations that can elucidate subsurface reservoir conditions and evaluate this potential water resource.
- Detailed petrography of CRBG units. Additional work to refine microscopic unit descriptions of mafic and opaque mineral percentages (point counts) for volcanic rocks will enhance existing descriptions of local CRBG units and may aid in distinguishing these aphyric units in the field.

ACKNOWLEDGMENTS

The global pandemic and wildfires of 2020 brought extraordinary challenges to our work and we were able to gratefully persevere because of the help of countless people. We thank, of CWU: Nick Zentner, Logan Wetherell, and many faculty of the Geology Department for many meaningful conversations and socially distanced field trips. Of WGS, thanks to: Alex Steely, Todd Lau, Will Gallin, Michael Polenz, and many others for insightful reviews of findings. Also of WGS, thanks to Stefanie Yourex and Rachel Noonan for acquiring and shipping personal protective equipment (PPE) to keep us all safer and healthy. Of USGS, we thank Steve Angster and Lydia Staisch for help synthesizing past and on-going regional work. Of emeritus investigators, we thank Steve Reidel and Jack Powell for clarifying structural and stratigraphic questions. Of WSU, thanks to Ashley Steiner, John Wolff and the whole staff at the WSU Peter Hooper GeoAnalytical lab in Pullman, WA for analyzing geochemistry samples and classifying CRBG rocks using their Machine Learning (ML) model. Also of WSU, thanks to Jeff Vervoort and Vic Valencia (ZirChron LLC) for analyzing our detrital zircon samples in the Radiogenic Isotope and Geochronology Laboratory. Of private citizens, thanks to the Charltons, Mays, Moores, Seferas, and other families along with countless other private landowners and businesses for land access. And Happy's Market for their delicious belly-filling breakfast burritos: big fan.

REFERENCES

- Allmendinger, R. W.; Cardozo, Nestor; Fisher, D. M., 2012, Structural geology algorithms: Vectors and tensors: Cambridge University Press, 289 p.
- Bentley, R. D., 1977, Stratigraphy of the Yakima basalts and structural evolution of the Yakima ridges in the western Columbia Plateau. In Brown, E. H.; Ellis, R. C., editors, Geology excursions in the Pacific Northwest: Geological Society of America Annual Meeting, p. 339–390.
- Black, L. P.; Kamo, S. L.; Allen, C. M.; Davis, D. W.; Aleinikoff, J. N.; Valley, J. W.; Mundil, Roland; Campbell, I. H.; Korsch, R. J.; Williams, I. S.; Foudoulis, Chris, 2004, Improved $^{206}\text{Pb}/^{218}\text{U}$ microprobe geochronology by the monitoring of a trace-element-related matrix effect; SHRIMP, ID-TIMS, ELA-ICP-MS and oxygen isotope documentation for a series of zircon standards: Chemical Geology, v. 205, no. 1–2, p. 115–140. [<https://doi.org/10.1016/j.chemgeo.2004.01.003>]
- Blakely, R. J.; Sherrod, B. L.; Weaver, C. S., 2020a, High-resolution aeromagnetic survey of the Wenatchee area, Washington: U.S. Geological Survey data release. [<https://doi.org/10.5066/P9EURKIG>]
- Blakely, R. J.; Sherrod, B. L.; Weaver, C. S., 2020b, High-resolution aeromagnetic survey of the Cle Elum area, Washington: U.S. Geological Survey data release. [<https://doi.org/10.5066/P9C9MADW>]
- Brocher, T. M.; Wells, R. E.; Lamb, A. P.; Weaver, C. S., 2017, Evidence for distributed clockwise rotation of the crust in the northwestern United States from fault geometries and focal mechanisms: Tectonics, v. 36, no. 5, p. 787–818. [<https://doi.org/10.1002/2016TC004223>]
- Cardozo, Nestor; Allmendinger, R. W., 2013, Spherical projections with OSXStereonet: Computers & Geosciences, v. 51, p. 193–205. [<https://doi.org/10.1016/j.cageo.2012.07.021>]
- Chang, Zhaoshan; Vervoort, J. D.; McClelland, W. C.; Knaack, Charles, 2006, U-Pb dating of zircon by LA-ICP-MS: Geochemistry, Geophysics, Geosystems, v. 7, no. 5, 14 p. [<https://doi.org/10.1029/2005GC001100>]

- Chiba, Tatsuro; Kaneta, Shin-ichi; Suzuki, Yusuke, 2008, Red relief image map: New visualization method for three dimensional data: The International Archives of the Photogrammetry, Remote Sensing and Spatial Information Sciences, v. 37, no. B2, p. 1071–1076.
- Czajkowski, J. L.; Bowman, J. D.; Schuster, J. E.; Wheeler, C. M., 2012, Oil and gas wells in Washington State: Washington Division of Geology and Earth Resources Open File Report 2012-02 (rev. 2015), 4 p., 1 Microsoft Excel file with 4 p. text. [http://www.dnr.wa.gov/Publications/ger_ofr2012-02_oil_and_gas_wells.zip]
- Ebinghaus, Alena; Jolley, D. W.; Hartley, A. J., 2015, Extrinsic forcing of plant ecosystems in a large igneous province: The Columbia River flood basalt province, Washington State, USA: *Geology*, v. 43, no. 12, p. 1107–1110. [<https://doi.org/10.1130/G37276.1>]
- Eddy, M. P.; Bowring, S. A.; Umhoefer, P. J.; Miller, R. B.; McLean, N. M.; Donaghy, E. E., 2016, High-resolution temporal and stratigraphic record of Siletzia's accretion and triple junction migration from nonmarine sedimentary basins in central and western Washington: *Geological Society of America Bulletin*, v. 128, no. 3–4, p. 425–441. [<https://doi.org/10.1130/B31335.1>]
- Eddy, M. P.; Umhoefer, P. J.; Miller, R. B.; Donaghy, E. E.; Gundersen, Melissa; Senes, F. I., 2017, Sedimentary, volcanic, and structural processes during triple-junction migration: Insights from the Paleogene record in central Washington. *In* Haugerud, R. A.; Kelsey, H. M., editors, *From the Puget Lowland to east of the Cascade Range: Geologic Excursions in the Pacific Northwest*: Geological Society of America Field Guide 49, p. 143–174. [[https://doi.org/10.1130/2017.0049\(07\)](https://doi.org/10.1130/2017.0049(07))]
- Eylon International, 2014a, Colockum 2014 project, Colockum Block Washington DNR Trust Lands lidar, collected between Jun. 25 and Jul. 6, 2014 by 3Di Geoterra, Inc., 3-ft resolution, accessed Aug. 31, 2020 [<http://lidarportal.dnr.wa.gov/>], metadata available on portal [ger_colockum_2014_lidar_report.pdf].
- Eylon International, 2014b, Colockum Extra 2014 project, Colockum Block Washington DNR Trust Lands lidar, collected by 3Di Geoterra, Inc., 3-ft resolution, accessed Aug. 31, 2020 [<http://lidarportal.dnr.wa.gov/>], no metadata available.
- FEMA, 2011, Kittitas FEMA 2011 project, Kittitas County, Washington CID 53037C lidar, collected between Apr. 17 and Apr. 19, 2011 by Watershed Sciences, Inc., 3-ft resolution, accessed Aug. 31, 2020 [<http://lidarportal.dnr.wa.gov/>], metadata available on portal [ger_kittitas_fema_2011_lidar_report.pdf].
- Hammond, P. E., 2013, Distribution, stratigraphy, and structure of the Grande Ronde Basalt in the upper Naches River basin, Yakima and Kittitas Counties, Washington. *In* Reidel, S. P.; Camp, V. E.; Ross, M. E.; Wolff, J. A.; Martin, B. S.; Tolan, T. L.; Wells, R. E., editors, *The Columbia River flood basalt province*: Geological Society of America Special Paper 497, p. 363–400. [[https://doi.org/10.1130/2013.2497\(15\)](https://doi.org/10.1130/2013.2497(15))]
- Heiskanen, W. A.; Meinesz, F. A. V., 1958, *Earth and its gravity field*: McGraw-Hill, 470 p.
- Hoyt, C. L., 1961, The Hammond sill—An intrusion in the Yakima Basalt near Wenatchee, Washington: *Northwest Science*, v. 35, no. 2, p. 58–64.
- Jachens, R. C.; Roberts, C. R., 1981, Documentation of a FORTRAN program, 'isocomp', for computing isostatic residual gravity: U.S. Geological Survey Open-File Report 81-574, 26 p. [<https://doi.org/10.3133/ofr81574>]
- Johnson, S. Y., 1985, Eocene strike-slip faulting and nonmarine basin formation in Washington. *In* Biddle, K. T.; Christie-Blick, Nicholas, editors, *Strike-slip deformation, basin formation, and sedimentation*: Society of Economic Paleontologists and Mineralogists Society for Sedimentary Geology Special Publication 37, p. 283–302. [<https://doi.org/10.2110/pec.85.37.0265>]
- Kaatz, M. R., 1959, Patterned ground in central Washington; A preliminary report: *Northwest Science*, v. 33, no. 4, p. 145–156.
- Kasbohm, Jennifer; Schoene, Blair, 2018, Rapid eruption of the Columbia River flood basalt and correlation with the mid-Miocene climate optimum: *Science Advances*, v. 4, no. 9, 8 p. [<https://doi.org/10.1126/sciadv.aat8223>]
- Kelsey, H. M.; Ladinsky, T. C.; Staisch, Lydia; Sherrod, B. L.; Blakely, R. J.; Pratt, T. L.; Stephenson, W. J.; Odum, J. K.; Wan, Elmira, 2017, The story of a Yakima fold and how it informs late Neogene and Quaternary backarc deformation in the Cascadia subduction zone, Manastash anticline, Washington, USA: *Tectonics*, v. 36, no. 10, p. 2085–2107. [<https://doi.org/10.1002/2017TC004558>]
- Lanphere, M. A.; Baadsgaard, Halfdan, 2001, Precise K–Ar, ⁴⁰Ar/³⁹Ar, Rb–Sr and U/Pb mineral ages from the 27.5 Ma Fish Canyon Tuff reference standard: *Chemical Geology*, v. 175, no. 3–4, p. 653–671. [[https://doi.org/10.1016/S0009-2541\(00\)00291-6](https://doi.org/10.1016/S0009-2541(00)00291-6)]
- Ludwig, K. R., 2012, User's manual for Isoplot 3.75: A geochronological toolkit for Microsoft Excel: Berkeley Geochronology Center Special Publication no. 5, 75 p. [https://www.geocalculate.com/wp-content/uploads/2019/10/Isoplot3_75-4_15manual.pdf]
- McCaffrey, Robert; King, R. W.; Payne, S. J.; Lancaster, Matthew, 2013, Active tectonics of northwestern U. S. inferred from GPS-derived surface velocities: *Journal of Geophysical Research Solid Earth*, v. 118, no. 2, p. 709–723. [<https://doi.org/10.1029/2012JB009473>]
- McDonald, E. V.; Busacca, A. J., 1992, Late Quaternary stratigraphy of loess in the Channeled Scabland and Palouse regions of Washington State: *Quaternary Research*, v. 38, no. 2, p. 141–156. [[https://doi.org/10.1016/0033-5894\(92\)90052-K](https://doi.org/10.1016/0033-5894(92)90052-K)]
- McMillan, Kent; Long, P. E.; Cross, R. W., 1989, Vesiculation in Columbia River basalts. *In* Reidel, S. P.; Hooper, P. R., editors, *Volcanism and tectonism in the Columbia River flood-basalt province*: Geological Society of America Special Paper 239, p. 157–167. [<https://doi.org/10.1130/SPE239-p157>]
- Morelli, Carlo; Gantar, C.; Honkasalo, Tauno; McConnel, R. K.; Tanner, J. G.; Szabo, Bela; Uotila, Urho; Whalen, C. T., 1974, The international gravity standardization net 1971 (IGSN71): International Association of Geodesy Special Publication No. 4, 194 p.
- Owens, Ron, 1995, The hydrology of the Kittitas Valley, Washington: Central Washington University Master of Science thesis, 205 p., 6 plates.
- Paces, J. B.; Miller Jr, J. D., 1993, Precise U–Pb ages of Duluth Complex and related mafic intrusions, northeastern Minnesota: Geochronological insights to physical, petrogenetic, paleomagnetic, and tectonomagmatic processes associated with the 1.1 Ga Midcontinent Rift System: *Journal of Geophysical Research Solid Earth*, v. 98, no. B8, p. 13997–14013. [<https://doi.org/10.1029/93JB01159>]
- Paton, Chad; Hellstrom, John; Paul, Bence; Woodhead, Jon; Hergt, Janet, 2011, Iolite: Freeware for the visualisation and processing of mass spectrometric data: *Journal of Analytical Atomic Spectrometry*, v. 26, no. 11, p. 2508–2518. [<https://doi.org/10.1039/C1JA10172B>]
- PSLC, 2011, Kittitas 2011 project, Kittitas, WA – Colockum Study Area lidar, collected between Sep. 15 and Nov. 5, 2010 by Watershed Sciences Inc., 3-ft resolution, accessed June 2020, [<http://lidarportal.dnr.wa.gov/>], metadata available on portal [ger_kittitas_2011_lidar_report.pdf].
- Porter, S. C., 1976, Pleistocene glaciation in the southern part of the north Cascade Range, Washington: *Geological Society of America Bulletin*, v. 87, no. 1, p. 61–75. [[https://doi.org/10.1130/0016-7606\(1976\)87<61:PGITSP>2.0.CO;2](https://doi.org/10.1130/0016-7606(1976)87<61:PGITSP>2.0.CO;2)]
- Reidel, S. P., 2005, A lava flow without a source: The Cohasset flow and its compositional components, Sentinel Bluffs Member, Columbia River Basalt Group: *Journal of Geology*, v. 113, no. 1, p. 1–21. [<https://doi.org/10.1086/425966>]
- Reidel, S. P., 2015, Igneous rock associations 15. The Columbia River Basalt Group: A flood basalt province in the Pacific Northwest, USA: *Geoscience Canada*, v. 42, no. 1, p. 151–168.

- Reidel, S. P.; Camp, V. E.; Tolan, T. L.; Martin, B. S., 2013a, The Columbia River flood basalt province: Stratigraphy, areal extent, volume, and physical volcanology. *In* Reidel, S. P.; Camp, V. E.; Ross, M. E.; Wolff, J. A.; Martin, B. S.; Tolan, T. L.; Wells, R. E., editors, The Columbia River flood basalt province: Geological Society of America Special Paper 497, p. 1–44. [https://doi.org/10.1130/2013.2497(01)]
- Reidel, S. P.; Camp, V. E.; Tolan, T. L.; Kauffman, J. D.; Garwood, D. L., 2013b, Tectonic evolution of the Columbia River flood basalt province. *In* Reidel, S. P.; Camp, V. E.; Ross, M. E.; Wolff, J. A.; Martin, B. S.; Tolan, T. L.; Wells, R. E., editors, The Columbia River flood basalt province: Geological Society of America Special Paper 497, p. 293–324. [https://doi.org/10.1130/2013.2497(12)]
- Reidel, S. P.; Scott, G. R.; Bazard, D. R.; Cross, R. W.; Dick, Brian, 1984, Post-12 million year clockwise rotation in the central Columbia Plateau, Washington: Tectonics, v. 3, no. 2, p. 251–273. [https://doi.org/10.1029/TC003i002p00251]
- Reidel, S. P.; Tolan, T. L., 2013, The Grande Ronde Basalt, Columbia River Basalt Group. *In* Reidel, S. P.; Camp, V. E.; Ross, M. E.; Wolff, J. A.; Martin, B. S.; Tolan, T. L.; Wells, R. E., editors, The Columbia River flood basalt province: Geological Society of America Special Paper 497, p. 117–154. [https://doi.org/10.1130/2013.2497(05)]
- Rosenmeier, F. J., 1968, Stratigraphy and structure of the Table mountain–Mission Peak area in the Wenatchee Mountains, central Washington: University of Washington Master of Science thesis, 44 p., 1 plate.
- Sadowski, A. J.; McCosby, J. B.; Anderson, M. L.; Lau, T. R.; Steiner, Ashley; DuFrane, S. A.; Rittenour, Tammy; Housen, Bernard, 2020, Geologic map of the Ellensburg North and southern half of the Reecer Canyon 7.5-minute quadrangles, Kittitas County, Washington: Washington Geological Survey Map Series 2020-01, 1 sheet, scale 1:24,000, 25 p. text. [http://www.dnr.wa.gov/publications/ger_ms2020-01_geol_map_ellensburg_north_reecer_canyon_24k.zip]
- Schmincke, Hans-Ulrich, 1964, Petrology, paleocurrents, and stratigraphy of the Ellensburg Formation and interbedded Yakima Basalt flows, south-central Washington: Johns Hopkins University Doctor of Philosophy thesis, 426 p.
- Schmincke, Hans-Ulrich, 1967, Stratigraphy and petrography of four upper Yakima Basalt flows in south-central Washington: Geological Society of America Bulletin, v. 78, no. 11, p. 1385–1422. [https://doi.org/10.1130/0016-7606(1967)78[1385:SAPOFU]2.0.CO;2]
- Sláma, Jiří; Košler, Jan; Condon, D. J.; Crowley, J. L.; Gerdes, Alex; Hanchar, J. M.; Horstwood, M. S. A.; Morris, G. A.; Nasdala, Lutz; Norberg, Nicholas; Schaltegger, Urs; Schoene, Blair; Tubrett, M. N.; Whitehouse, M. J., 2018, Plešovice zircon—A new natural reference material for U-Pb and Hf isotopic microanalysis: Chemical Geology, v. 249, no. 1–2, p. 1–35. [https://doi.org/10.1016/j.chemgeo.2007.11.005]
- Smith, G. A., 1988a, Neogene synvolcanic and syntectonic sedimentation in central Washington: Geological Society of America Bulletin, v. 100, no. 9, p. 1479–1492. [https://doi.org/10.1130/0016-7606(1988)100<1479:NSASSI>2.3.CO;2]
- Smith, G. A., 1988b, Sedimentology of proximal to distal volcanics dispersed across an active foldbelt: Ellensburg Formation (late Miocene), central Washington: Sedimentology, v. 35, no. 6, p. 953–977. [https://doi.org/10.1111/j.1365-3091.1988.tb01740.x]
- Staisch, Lydia; Blakely, Richard; Kelsey, Harvey; Styron, Richard; Sherrod, Brian, 2018a, Crustal structure and Quaternary acceleration of deformation rates in central Washington revealed by stream profile inversion, potential field geophysics, and structural geology of the Yakima folds: Tectonics, v. 37, no. 6, p. 1750–1770. [https://doi.org/10.1029/2017TC004916]
- Staisch, Lydia; Kelsey, Harvey; Sherrod, Brian; Möller, Andreas; Paces, James; Blakely, Richard; Styron, Richard, 2018b, Miocene–Pleistocene deformation of the Saddle Mountains: Implications for seismic hazard in central Washington, USA: Geological Society of America Bulletin, v. 130, no. 3–4, p. 411–437. [https://doi.org/10.1130/B31783.1]
- Swick, C. H., 1942, Pendulum gravity measurements and isostatic reductions: U.S. Department of Commerce Coast and Geodetic Survey Special Publication 232, 82 p.
- Tabor, R. W.; Waitt, R. B., Jr.; Frizzell, V. A., Jr.; Swanson, D. A.; Byerly, G. R.; Bentley, R. D., 1982, Geologic map of the Wenatchee 1:100,000 quadrangle, central Washington: U.S. Geological Survey Miscellaneous Investigations Series Map I-1311, 1 sheet, scale 1:100,000, with 26 p. text. [https://doi.org/10.3133/i1311]
- Telford, W. M.; Geldart, L. O.; Sheriff, R. E., 1990, Applied Geophysics: Cambridge University Press, 770 p.
- UNAVCO, 2014, Yakima 2008 project, Southern California and Washington (Yakima) Fault Systems LiDAR Survey, collected on Apr. 26, 2008 by NCALM, 3-ft resolution, accessed Aug. 31, 2020 [http://lidarportal.dnr.wa.gov/], metadata available on portal [ger_yakima_2008_lidar_project_report.pdf].
- WA DNR, 2018a, Yakima Basin 2018 project, Yakima Basin Washington LiDAR, collected between Nov. 17, 2017 and May 23, 2018 by Quantum Spatial, Inc., 3-ft resolution, accessed Aug. 31, 2020 [http://lidarportal.dnr.wa.gov/], metadata available on portal [ger_yakima_basin_2018_lidar_report.pdf].
- WA DNR, 2018b, Yakima Basin North 2018 project, Yakima Basin Wildfire Division Washington, collected between Jul. 24 and Sep. 2, 2018 by Quantum Spatial, Inc., 3-ft resolution, accessed Aug. 31, 2020 [http://lidarportal.dnr.wa.gov/], metadata available on portal [ger_yakima_basin_north_2018_lidar_report.pdf].
- Waitt, R. B., Jr., 1979, Late Cenozoic deposits, landforms, stratigraphy, and tectonism in Kittitas Valley, Washington: U.S. Geological Survey Professional Paper 1127, 18 p. [https://doi.org/10.3133/pp1127]
- Wells, R. E.; McCaffrey, Robert, 2013, Steady rotation of the Cascade arc: Geology, v. 41, no. 9, p. 1027–1030. [https://doi.org/10.1130/G34514.1]
- Wells, R. E.; Weaver, C. S.; Blakely, R. J., 1998, Fore-arc migration in Cascadia and its neotectonic significance: Geology, v. 26, no. 8, p. 759–762. [https://doi.org/10.1130/0091-7613(1998)026<0759:FAMICA>2.3.CO;2]
- Wiedenbeck, M.; Allé, P.; Corfu, F.; Griffin, W. L.; Meier, M.; Oberli, F.; Von Quadt, A.; Roddick, J. C.; Spiegel, W., 1995, Three natural zircon standards for U-Th-Pb, Lu-Hf, trace element and REE analyses: Geostandards Newsletters, v. 19, no. 1, p. 1–23. [https://doi.org/10.1111/j.1751-908X.1995.tb00147.x]
- Williams, I. S., 1997, U-Th-Pb geochronology by ion microprobe. *In* McKibben, M. A.; Shanks III, W. C.; Ridley, W. I., editors, Applications of microanalytical techniques to understanding mineralizing processes: Reviews in Economic Geology, v. 7, p. 1–32. [https://doi.org/10.5382/Rev.07.01]
- Williams, Howel; Masson, P. H., 1949, Geology of the Macdoel quadrangle and circular soil structures in northeastern California: California Division of Mines and Geology, Bulletin 151, scale 1:125,000. [https://ngmdb.usgs.gov/Prodesc/proddesc_531.htm]

Appendix A. Detrital Zircon Separation and Analytical Methods

Zircon separates were extracted from three samples in the map area by ZirChron LLC in Tucson, AZ. Two zircon separates came from samples that had weights between 4 to 10 kg and one zircon separate came from a pumice separate that weighed less than 100 g. Each sample was individually unpacked and pressure washed with water to remove any debris and (or) foreign material. Sample rock fragments were placed in the sample chamber of an Electro Pulse Disaggregator (EPD, Marx generator), then electrical pulses were applied at 1 Hz with discharges of ~250 kV for 15 minutes. Sample material that passed through the 500 μm stainless steel mesh sieve was collected in a disposable plastic bag. The coarser material remaining in the crush chamber was collected, dried, and if necessary, a rock crusher or pulverizer was used to reduce grain size. The collected (<500 μm) material was sieved a second time through 350 μm and 25 μm nylon disposable mesh sieves. The fraction of material >350 μm was added to the 500 μm material and material smaller than 25 μm was discarded. Material between 350 μm and 25 μm was then processed following traditional methods using the Wilfley water table, Frantz paramagnetic separator, and two-step (3.00 g/cm³ and 3.32 g/cm³) heavy liquid MEI separations.

From each zircon separate, ~100 individual zircon grains were hand selected and mounted in epoxy. The grain mounts were polished to expose the grain centers, and regions suitable for analysis were identified from optical imaging. Zircon U-Pb ages from the map area were measured at the Radiogenic Isotope and Geochronology Lab (RIGL) at Washington State University using an Analyte G2 193 excimer laser ablation system coupled with a Thermo-Finnigan Element 2 single-collector inductively coupled plasma mass spectrometer. The laser parameters were 25 μm in diameter spot size, 10 Hz repetition rate, and ~5.0 J/cm² fluence. For the U-Pb measurement, we mostly followed the method of Chang and others (2006), except for the use of the 193 nm laser system instead of the 213 nm laser. A 10-second blank measurement of the He and Ar carrier gases (Laser off) before each analysis was followed by 250 scans across masses ²⁰²Hg, ²⁰⁴Pb+Hg, ²⁰⁶Pb, ²⁰⁷Pb, ²⁰⁸Pb, ²³²Th, ²³⁵U, and ²³⁸U during ~30-sec-long laser ablation periods (in other words, one continuous, 30-second ablation at 10 Hz—10 shots fired per second—for ~300 laser shots). Analyses of zircon unknowns, standards, and quality control zircon grains were interspersed with analyses of external calibration standards, typically with 10–12 unknowns bracketed by multiple analyses of two different zircon standards (Plešovice and FC-1). The Plešovice standard (337 Ma; Sláma and others, 2018) was used to calibrate the ²⁰⁶Pb/²³⁸U and ²⁰⁷Pb/²³⁵U ages, and the FC-1 standard (1,099 Ma; Paces and Miller, 1993) was used for calibration of ²⁰⁷Pb/²⁰⁶Pb ages owing to its high count rate for ²⁰⁷Pb (~2–4 times higher than that of Plešovice). Zircon 91500 (1,065 Ma; Wiedenbeck and others, 1995; n=28 ²⁰⁷Pb/²⁰⁶Pb age=1,063 +2.4/-5.0 Ma), Fish Canyon Tuff (~27.5 Ma Lanphere and Baadsgaard, 2001; n=35 ²⁰⁶Pb/²³⁸U age=27.9 +0.1/-0.2 Ma) and Temora2 (417 Ma; Black and others, 2004, n=48 ²⁰⁶Pb/²³⁸U age=417.0 +1/-1 Ma) were used as quality control standards. Data were processed offline using the Iolite software (Paton and others, 2011). Common lead (Pb) correction was performed using the ²⁰⁷Pb method (Williams, 1997). Plots were calculated using Isoplot 4.16 (Ludwig, 2012). Zircon U-Pb data are reported in Table DS02A through DS02C.